Coordination Chemistry Reviews 539 (2025) 216751

Contents lists available at ScienceDirect

Coordination Chemistry Reviews

journal homepage: www.elsevier.com/locate/ccr

Review

Recent trends and prospects in electrochemical nitrate reduction to ammonia with an emphasis on cobalt catalysts

Gaihong Wang [a,b], Zhijie Chen [b,*], Jiangzhou Xie [c], Lei Ding [d], Jinliang Zhu [e], Wei Wei [a,*], Yi-Ming Yan [f], Dewei Chu [g], Bing-Jie Ni [b,*]

[a] Centre for Technology in Water and Wastewater, School of Civil and Environmental Engineering, University of Technology Sydney, Sydney, NSW 2007, Australia
[b] UNSW Water Research Centre, School of Civil and Environmental Engineering, The University New South Wales, Sydney, NSW 2052, Australia
[c] School of Mechanical and Manufacturing Engineering, University of New South Wales, Sydney, New South Wales 2052, Australia
[d] Centre for Atomaterials and Nanomanufacturing, School of Science, RMIT University, Melbourne, Victoria 3000, Australia
[e] School of Resources, Environment and Materials, State Key Laboratory of Featured Metal Materials and Life-cycle Safety for Composite Structures, Guangxi University, Nanning 530004, PR China
[f] State Key Lab of Organic–Inorganic Composites, Beijing Advanced Innovation Center for Soft Matter Science and Engineering, Beijing University of Chemical Technology, Beijing 100029, PR China
[g] School of Materials Science and Engineering, The University of New South Wales, Sydney, NSW 2052, Australia

ARTICLE INFO

Keywords:
Electrochemical nitrate reduction
Catalyst design
Ammonia
Electrocatalysts
Catalytic mechanisms

ABSTRACT

Ammonia is gaining recognition as a promising energy carrier due to its high energy density, ease of liquefaction, and existing robust production and distribution infrastructure, particularly within the agricultural sector. The electrochemical nitrate reduction reaction (NO_3RR), conducted under ambient conditions, offers a sustainable alternative to the energy-intensive Haber–Bosch (H—B) process, addressing both environmental and energy challenges. Recent advancements in understanding catalytic mechanisms, optimizing catalytic systems, and designing advanced catalysts have substantially enhanced the efficiency of nitrate-to-ammonia conversion. Among these, cobalt (Co)-based electrocatalysts have emerged as a cost-effective and efficient alternative to noble metals, owing to their earth abundance, low cost, and favorable catalytic properties. This review provides a comprehensive overview of recent progress in NO_3RR, emphasizing Co-based electrocatalysts. It delves into NO_3RR mechanism analysis, critical considerations for system optimization, and innovative Co-based catalyst design strategies. Additionally, we explore current challenges and propose future directions for improving Co-based electrocatalyst performance, aiming to advance the rational design of efficient catalysts for sustainable ammonia synthesis.

1. Introduction

Nitrate (NO_3^-) is a key nitrogen-containing compound, essential for plant growth and soil fertility within the nitrogen cycle [1]. However, excessive use of nitrogen-based fertilizers in agriculture can lead to nitrate leaching into groundwater and surface water bodies, resulting in eutrophication and harming aquatic life [2,3]. Moreover, increased nitrate concentrations in drinking water have been linked to methemoglobinemia, commonly referred to as “blue baby syndrome,” which impairs oxygen transport in the blood [4]. Given the potential detrimental effects of nitrate pollution on ecosystems and human health, addressing it is imperative. Efforts to mitigate nitrate pollution typically focus on two main approaches: separating nitrates from water and transforming them into harmless or valuable compounds. Various separation technologies are employed for removing nitrates, including reverse osmosis [5], ion exchange [6], adsorption [7], and electrodialysis [8]. Despite being favored for their simplicity and cost-effectiveness, physical separation methods still encounter challenges such as fouling, scaling, and the need for post-treatment steps [9–11]. On the other hand, nitrate conversion methods involve biological denitrification [12], chemical catalytic reduction [13], electrocatalytic reduction [14], and photocatalytic processes [15]. While these methods can achieve high nitrate conversion efficiency and reduce post-treatment costs compared to separation technologies, they still have drawbacks. For instance, biological denitrification is pH-dependent and time-consuming, chemical catalytic methods incur high operational costs, and photocatalysis

* Corresponding authors.
E-mail addresses: zhijie.chen1@unsw.edu.au (Z. Chen), wei.wei@uts.edu.au (W. Wei), bingjieni@gmail.com (B.-J. Ni).

https://doi.org/10.1016/j.ccr.2025.216751
Received 29 December 2024; Received in revised form 8 April 2025; Accepted 19 April 2025
Available online 28 April 2025

exhibits low stability. In contrast, electrocatalytic reduction emerges as a promising approach due to its advantages in green chemistry, versatility, and scalability [16,17]. Electrochemical processes could efficiently reduce nitrates to harmless nitrogen gas (N_2) or valuable compounds like ammonia (NH_3), offering a more sustainable solution to nitrate pollution.

Ammonia is a crucial chemical in modern agriculture and industry, primarily due to its extensive use in fertilizers, which are essential for maintaining soil fertility and supporting global food production [18]. Beyond its agricultural importance, ammonia is the focus of ongoing research as a possible energy carrier due to its remarkable energy density and the ability to store and transport hydrogen in a stable form, contributing to sustainable energy solutions [19]. Ammonia is traditionally synthesized through the Haber-Bosch process, despite its effectiveness, highly energy-consuming and contributing substantially to greenhouse gas emissions [20]. This process operates at high temperatures and pressures, consuming about 1–2 % of global energy stock and producing large quantities of CO_2 [21]. In contrast, electrochemical methods for ammonia synthesis offer several advantages, including lower energy consumption, milder operating conditions, and the potential for integration with renewable energy sources, thus reducing the overall carbon footprint [22].

During the NO_3RR, nitrate ions undergo reduction at the cathode while the oxygen evolution reaction typically occurs at the anode. This process can induce the generation of multiple products, with energetically stable N_2 and NH_3 being the primary ones. The reaction processes are described by the following equations: [14,23].

$$2NO_3^- + 12H^+ + 10e^- \longrightarrow N_2 + 6H_2O \; E^0 = 1.17 \text{ V vs.SHE} \quad (1)$$

$$NO_3^- + 9H^+ + 8e^- \longrightarrow NH_3 + 3H_2O \; E^0 = -0.12 \text{ V vs.SHE} \quad (2)$$

The reduction of nitrate to N_2 involves N—N bond assembly via a second-order mechanism, which faces competition from reactions with first-order kinetics to produce alternative products like NH_3 or hydroxylamine (NH_2OH), thereby impacting the selectivity of the reaction [24]. Despite reducing nitrate to ammonia requires two more electrons compared to N_2, the catalytic process for nitrate reduction to ammonia is generally more promising. This is because the N—N bond generation, which is necessary for N_2 emergence, is energetically less advantageous than the reactions yielding [25,26]. Furthermore, the conversion of nitrate into ammonia (Eq. 2) requires a lower standard reduction potential, making it thermodynamically favorable under certain conditions [27]. Notably, ammonia has gained attention as a potential energy carrier owing to its high storage capacity and ease of liquefaction, making it a promising candidate for storing and transporting hydrogen [28]. Overall, achieving selective ammonia synthesis via nitrate electroreduction is crucial for both the nitrate pollution remediation and sustainable ammonia supply.

While electrochemically reducing nitrate to ammonia, it is indispensable to avoid the formation of environmentally benign N_2 and harmful offshoots like nitric oxide (NO), nitrite (NO_2^-), and nitrous oxide (N_2O) [29]. Additionally, minimizing the competitive hydrogen evolution reaction (HER) is essential to maximizing the yield of ammonia [30]. The selectivity of the electrochemical nitrate reduction process towards NH_3 can be influenced by various factors including reaction conditions (such as pH and temperature), electrolyte composition, and electrode catalysts [31–36]. Catalyst materials play a critical role in achieving high selectivity towards ammonia, as well as high efficiency. Various types of electrocatalysts have been explored for this purpose, including novel metals, transition metals, and carbon-based materials [37–40]. The comparative analysis of different electrocatalysts for NO_3RR reveals notable differences in performance across key parameters such as activity, NH_3 selectivity, cost-effectiveness, stability, and HER suppression. As illustrated in the radar chart (Fig. 1a), Co-based electrocatalysts demonstrate a unique balance of high NH_3 selectivity, moderate cost-effectiveness, and good stability, positioning it as a promising candidate for efficient and sustainable ammonia synthesis. In comparison, Fe-based electrocatalysts exhibit the highest cost-effectiveness due to its low cost and abundance, but its moderate activity and selectivity limit its overall efficiency [41,42]. Cu-based electrocatalysts show moderate cost-effectiveness and competitive NH_3 selectivity, but it struggles with stability issues due to the formation of passivation layers under alkaline conditions [43,44]. Novel metal electrocatalysts (e.g., Pt, Pd, Rh, and Au) provide high activity but suffer from low cost-effectiveness due to their high cost and scarcity [45–47]. Metal-free electrocatalysts excel in HER suppression performance and cost-effectiveness, yet they exhibit lower activity and stability for NO_3RR [48,49]. Furthermore, theoretical and experimental studies both provided strong evidence for the outstanding performance of Co-based catalysts over other catalysts. Theoretical calculations indicated that Co_3O_4 exhibited an ultralow rate-determining free energy change, suggesting superior catalytic activity for NO_3RR compared to metals such as Pd, Ni, Zn, Cu, Ru, Fe, and Rh. In addition, Wu et al. made a comparison of twelve common transition metal oxide catalysts under a high cathodic current density of 0.25 A cm^{-2}, wherein Co_3O_4 catalyst achieved the highest ammonia Faradaic efficiency (85.15 %) and moderate activity (−0.25 V vs. Reversible hydrogen electrode (RHE)) (Fig. 1b) [50].

Despite notable progress (see Table 1), challenges such as improving selectivity, enhancing stability, and optimizing catalyst-support interfaces persist. Addressing these issues is essential for guiding the

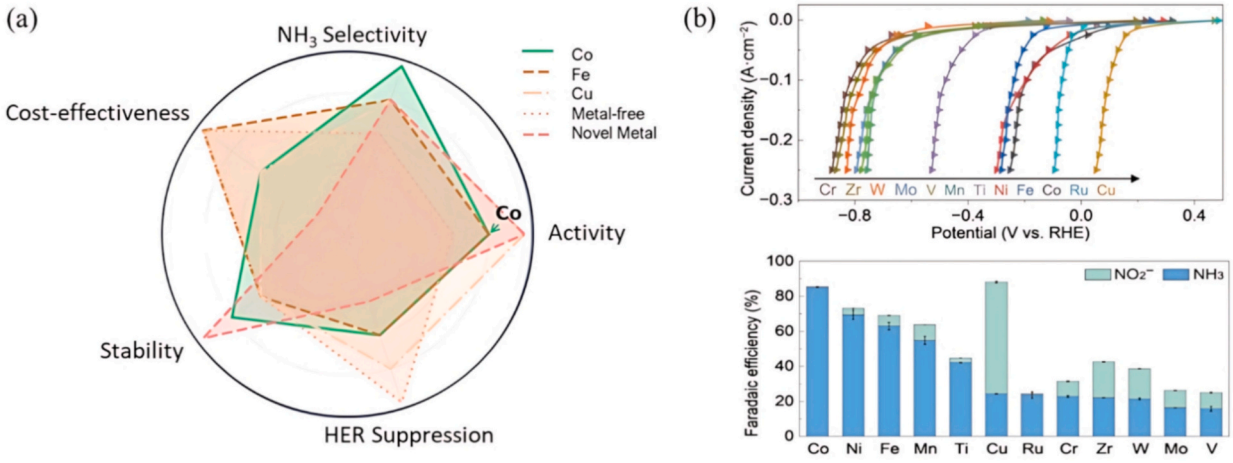

Fig.1. (a) The comparative analysis of different electrocatalysts for NO_3RR. (b) Polarization curves and faradaic efficiency of ammonia and nitrate production of twelve transition metal oxide catalysts. Reproduced with permission [50]. Copyright 2024, Springer Nature.

Table 1
Faradaic efficiency and yield rate of ammonia for various Co-based electrocatalysts in NO_3RR.

Catalysts	Electrolyte	Applied Potential /V vs. RHE	Ammonia Yield Rate	Ammonia Faradaic Efficiency/%	Ref.
Co_3O_4	0.1 M NaOH 0.1 M NO_3^-	−0.5	0.72 mmol h^{-1} cm^{-2}	96.90	[68]
Co_3O_4/Co	0.1 M Na_2SO_4 1000 ppm NO_3^-	−0.8	0.26 mmol h^{-1} cm^{-2}	88.70	[69]
Fe-Co_3O_4	0.1 M PBS 0.05 M NO_3^-	−0.7	36.47 mmol h^{-1} g^{-1}	95.50	[70]
Cu-Co_3O_4	0.1 M Na_2SO_4 500 ppm NO_3^-	−0.6	36.71 mmol h^{-1} g^{-1}	86.50	[71]
$CuCo_2O_4$	1 M KOH 0.1 M NO_3^-	−0.3	394.5 mmol h^{-1} g^{-1}	81.90	[72]
Co_2AlO_4	0.1 M PBS 0.1 M NO_3^-	−0.7	0.36 mmol h^{-1} cm^{-2}	92.60	[66]
Co_3O_4-Mn_x	0.5 M K_2SO_4 0.1 M NO_3^-	−0.6	0.7 mmol h^{-1} cm^{-2}	99.50	[73]
$NiCo_2O_4$	0.1 M NaOH 0.1 M NO_3^-	−0.3	0.45 mmol h^{-1} cm^{-2}	99.00	[67]
$FeCo_2O_4$	0.1 M NaOH 0.02 mM NO_3^-	−0.5	0.29 mmol h^{-1} cm^{-2}	95.90	[74]
$ZnCo_2O_4$	0.1 M NaOH 0.1 M NO_3^-	−0.6	0.63 mmol h^{-1} cm^{-2}	98.33	[75]
$CoMn_2O_4$/NC	0.1 M Na_2SO_4 0.1 M NO_3^-	−0.7	144.5 mmol h^{-1} g^{-1}	92.40	[76]
CoP	0.5 M Na_2SO_4 0.05 M NO_3^-	−0.5	1770 mmol h^{-1} g^{-1}	92.40	[77]
CoP	1 M NaOH 0.005 M NO_3^-	−0.4	0.018 mmol h^{-1} cm^{-2}	65.00	[62]
CoP	0.5 M K_2SO_4 0.05 M NO_3^-	−0.5	1134 mmol h^{-1} g^{-1}	94.00	[78]
CoP-CNS	1 M KOH 0.1 M NO_3^-	−0.63	1.6 mmol h^{-1} cm^{-2}	100.00	[56]
Fe/CoP NHs	1 M KOH 0.05 M NO_3^-	−0.25	1623 mmol h^{-1} g^{-1}	93.30	[79]
CoP/TiO_2	0.1 M NaOH 0.1 M NO_3^-	−0.3	0.5 mmol h^{-1} cm^{-2}	95.00	[80]
Co-P	0.2 M Na_2SO_4 200 ppm NO_3^-	−0.3	0.019 mmol h^{-1} cm^{-2}	95.00	[81]
CoP	1.0 M NaOH 1.0 M NO_3^-	−0.3	9560 mmol h^{-1} cm^{-2}	100.00	[61]
Co@NC	0.1 M NaOH 0.1 M NO_3^-	−0.5	500 mmol h^{-1} g^{-1}	96.50	[59]
Co/NC-800	0.1 M Na_2SO_4 0.1 M NO_3^-	−1.2	44 mmol h^{-1} g^{-1}	81.20	[60]
MR Co-NC	0.1 M KOH 0.1 M NO_3^-	−0.7	1.25 mmol h^{-1} cm^{-2}	95.35	[82]
CuCoSP	0.1 M KOH 0.1 M NO_3^-	−0.18	1.17 mmol h^{-1} cm^{-2}	90.60	[83]
Co@TiO_2	0.1 M PBS 0.1 M NO_3^-	−0.7	0.371 mmol h^{-1} cm^{-2}	96.70	[84]
$ZnCo_2O_4$	0.1 M KOH 0.1 M NO_3^-	−0.4	70 mmol h^{-1} g^{-1}	95.40	[85]
$Co_{1-x}Cu_x$	1 M KOH 0.05 M NO_3^-	−0.03	176 mmol h^{-1} g^{-1}	95.40	[86]
Co/PN-C	0.1 M NaOH 0.1 M NO_3^-	−0.2	1.41 mmol h^{-1} cm^{-2}	97.80	[87]
Co@CC	0.1 M NaOH 0.1 M NO_3^-	−0.8	0.60 mmol h^{-1} cm^{-2}	93.40	[88]
Co-NCNT	0.1 M NaOH 0.1 M NO_3^-	−0.6	0.35 mmol h^{-1} cm^{-2}	92.00	[89]
Co@JDC	0.1 M PBS 0.1 M NO_3^-	-1	2800 mmol h^{-1} g^{-1}	96.90	[90]
Co-CNF/ ZIF-CoP	1 M KOH 0.1 M NO_3^-	−0.6	2.26 mmol h^{-1} cm^{-2}	90.00	[91]
CoB@TiO_2	0.1 M Na_2SO_4 400 ppm NO_3^-	−0.70	0.23 mmol h^{-1} cm^{-2}	95.20	[92]
Co-CNP	0.02 M Na_2SO_4 100 ppm NO_3^-	−0.69	0.025 mmol h^{-1} cm^{-2}	92.00	[93]
Fe1/Cu2-Co_3O_4	0.2 M Na_2SO_4 100 ppm NO_3^-	−0.79	0.175 mmol h^{-1} cm^{-2}	98.46	[94]
PP-Co/CP	0.1 M NaOH 0.1 M NO_3^-	−0.6	1100 mmol h^{-1} g^{-1}	90.10	[95]
Co_3O_4-Mn_2	0.5 M K_2SO_4 0.1 M NO_3^-	−1.2	2.06 mmol h^{-1} cm^{-2}	99.50	[96]
CoO-NC/ graphene	1 M KOH 1 M NO_3^-	−0.75	25,630 mmol h^{-1} g^{-1}	98.00	[97]

rational design of next-generation Co-based catalysts, with the ultimate goal of advancing more efficient and environmentally friendly ammonia synthesis technologies. This review will delve into the up-to-date advancements in NO_3RR, focusing on Co-based electrocatalysts. By providing a comprehensive analysis of NO_3RR mechanisms, evaluating catalyst performance under various conditions, and summarizing design strategies for optimizing the catalytic sites of Co, this review seeks to offer deeper insights into optimizing electrocatalytic processes, enhancing catalyst efficiency, and guiding future developments in the field of nitrate reduction to ammonia.

2. Mechanistic understanding of NO_3RR

2.1. Reaction mechanisms of NO_3RR

Nitrate reduction is a multifaceted electrochemical process encompassing a series of nitrogen-containing species with valence states ranging from +5 to −3 [51]. This multifaceted reaction proceeds through multiple pathways, leading to the formation of various nitrogenous products. Among these, NH_3 is particularly favored thermodynamically, and the mechanisms involved in its formation have attracted significant research efforts. For Co-based catalysts, three main reaction pathways from NO_3^- to NH_3 have been summarized as shown in Fig. 2a. All three pathways involve an eight-electron transfer process, requiring sequential reduction and protonation steps [52,53]. Additionally, each pathway follows a progressive deoxygenation mechanism, where oxygen atoms are removed from nitrate through intermediates before reaching ammonia. Another common aspect is that hydrogenation plays a crucial role in determining the selectivity towards NH_3 versus undesired byproducts like N_2 or N_2O. Despite these similarities, the pathways exhibit distinct characteristics. The first pathway ($NO_3^- \rightarrow NO_3H \rightarrow NO_2 \rightarrow NO_2H \rightarrow NO \rightarrow NOH \rightarrow N/NHOH \rightarrow NH \rightarrow NH_2 \rightarrow NH_3$) involves stepwise deoxygenation and hydrogenation, making it the most complex route with potential side products like NO and N_2O. The second pathway ($NO_3^- \rightarrow NO_2 \rightarrow NO \rightarrow N \rightarrow NH \rightarrow NH_2 \rightarrow NH_3$) follows a more direct reduction process but increases the likelihood of N_2 formation. The third pathway ($NO_3^- \rightarrow NO_2 \rightarrow NO \rightarrow NOH \rightarrow NHOH \rightarrow NH_2OH \rightarrow NH_2$) utilizes hydroxylamine (NH_2OH) as a key intermediate, offering a selective route to NH_3 while reducing N_2 formation, though NH_2OH stability must be managed.

2.2. Key role of active hydrogen species (*H)

In the hydrogen-mediated nitrate reduction process, the crucial step is the Volmer step ($H_2O \rightarrow *H + *OH$). This critical step supplies *H, which serves as reducing agents to facilitate the transformation of adsorbed nitrate ($*NO_3$) into ammonia [54]. Furthermore, the selectivity of NH_3 critically depends on the availability and timely supply of *H atoms, highlighting the need to maintain a dynamic equilibrium of active hydrogen [55]. Maintaining this equilibrium ensures a steady flow of *H atoms, while avoiding an excess that could disrupt reaction kinetics or lead to side reactions. The study by Fan et al. provided deeper insights into this dynamic equilibrium through the comparison of two catalysts, Co and CoP, in the nitrate reduction process (Fig. 2b) [56]. Their findings showed that CoP, with its superior capacity for water splitting, generated more *H atoms than Co. This enhanced ability to

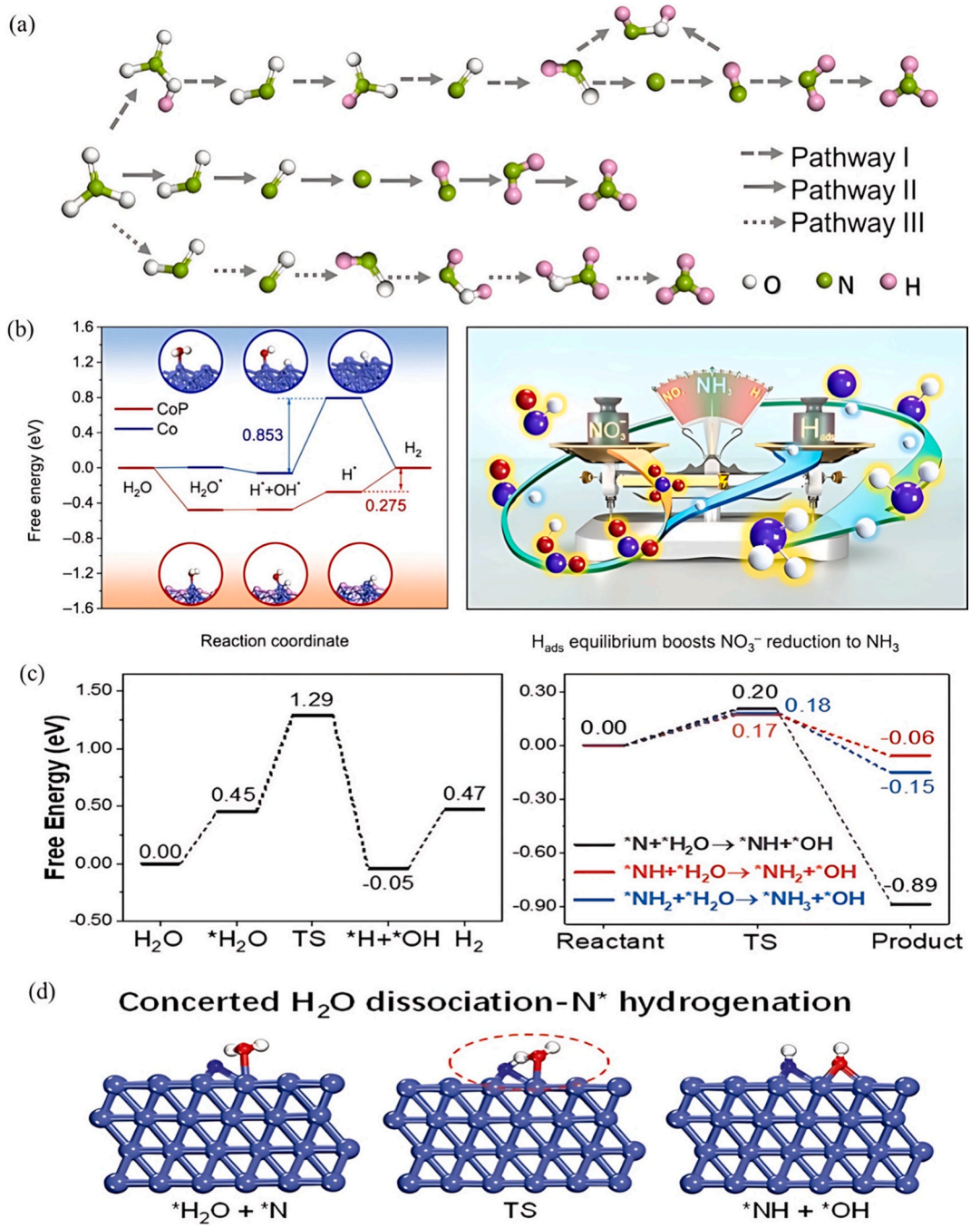

Fig.2. (a) Three main reaction pathways from NO_3^- to NH_3 for Co-based catalysts. (b) HER processes on CoP (211) and Co (111) surfaces, along with the proposed NO_3RR mechanism on CoP, are depicted. Colour scheme: Co in light blue, P in pink, H in white, O in red, and N in dark blue [56]. (c) Free energy profiles for intermediates on Co (111) in the HER pathway, incorporating the concerted H_2O dissociation and subsequent hydrogenation of *N, *NH, and *NH_2. (d) Proposed initial, transition, and final states for the reaction *N + *H_2O → *NH + *OH on Co (111) surface. Co, N, O, and H atoms are represented by light blue, blue, red, and white spheres, respectively [57]. (For interpretation of the references to colour in this figure legend, the reader is referred to the web version of this article.)

both produce and retain *H enabled CoP to facilitate a more efficient nitrate reduction, whereas Co, with its higher energy barrier for water decomposition, struggled to maintain the balance between *H generation and consumption.

While the hydrogenation process was mediated by *H, Deng et al. further elaborated that an novel balance mechanism between *H production and consumption involved the interaction between adsorbed hydrogen atoms and nucleophilic intermediates, such as *N, *NH, and *NH_2 [57]. Theoretical analysis revealed that the energy required for the reaction *NH_2 + *H_2O → *NH_3 + *OH was substantially reduced than that for the traditional Volmer step (H_2O → *H + *OH)(Fig. 2b). It indicated that, rather than relying on the slower water dissociation process, the hydrogenation of *N-based intermediates occurred simultaneously with water deprotonation, overcoming kinetic barriers and ensuring a steady supply of protons (Fig. 2d).

2.3. *Important considerations of NO_3RR system*

The electrochemical nitrate reduction reaction has gained significant attention as a sustainable method for mitigating nitrate pollution while

simultaneously recovering ammonia, a valuable chemical. However, the practical implementation of NO_3RR hinges on optimizing key factors such as the electrolyte environment and nitrate concentration. Additionally, integrating NO_3RR with coupled reaction systems presents an effective strategy to improve overall system efficiency. This section will explore the impact of these parameters on the behavior of cobalt-based catalysts, with a focus on enhancing selectivity, energy efficiency, and stability to achieve a more sustainable and efficient process.

2.3.1. Electrolyte pH

It is well known that the pH conditions can be regulated to tune the performance of NO_3RR, particularly with regards to the ammonia yield rate and Faradaic efficiency (FE). Yan et al. discovered that the priority reaction pathways, potential-determining steps, and limiting potentials of single-atom catalysts were influenced by pH, as shown by the adsorption free energies (G_{NO*} and G_{NH2*}), local atomic coordination and active site electronic configurations [58]. Alkaline electrolytes have consistently demonstrated superior performance in nitrate reduction. The high level of hydroxide ions (OH^-) in alkaline media enhances the adsorption and activation of NO_3^- at the catalyst surface, facilitating more effective electron transfer and the subsequent reduction of nitrates into ammonia. Alkaline conditions also stabilize key reaction intermediates, such as adsorbed hydrogen, thereby promoting the formation of ammonia while minimizing competing side reactions like HER. In contrast, neutral pH electrolytes, such as PBS or Na_2SO_4, generally show lower ammonia yields, due to increased competition between nitrate reduction and hydrogen evolution. The lack of OH^- hinders the efficient protonation of nitrate intermediates and increases the likelihood of undesired hydrogen evolution, reducing the availability of electrons for nitrate reduction. This ultimately slows the reaction kinetics, resulting in lower ammonia yields compared to alkaline conditions. For instance, the same Co single atom catalysts, such as Co@NC and Co/NC-800, achieved ammonia yield rates of 500 and 44 mmol h^{-1} g^{-1} in 0.1 M KOH and 0.1 M Na_2SO_4, respectively, with FE of 96.5 % and 88.2 % [59,60].

2.3.2. Nitrate concentration

The concentration of nitrate in the electrolyte is also essential to determining the performance of Co-based catalysts in nitrate reduction, directly affecting both ammonia yield rates and Faradaic efficiencies. A higher nitrate concentration enhances the availability of nitrate ions at the catalytic surface, facilitating electron transfer and accelerating reaction rates. This effect is particularly prominent in alkaline environments where hydroxide ions further promote catalytic activity by stabilizing reaction intermediates. For example, Ye et al. investigated the catalytic behavior of CoP catalyst in alkaline electrolyte (1.0 M $NaNO_3$ and 1.0 M NaOH) and obtained a very high ammonia yield efficiency of 9.56 mmol h^{-1} cm^{-2} and FE of 100 % [61]. The high concentration of nitrate ions ensured that the catalytic centers were continuously supplied with reactants, enabling efficient electron transfer for nitrate reduction. Furthermore, the presence of a high OH^- concentration in the alkaline medium aided in stabilizing key intermediates such as NO_3^- and NO_2^-, crucial for the multi-step reduction process to ammonia. This combination of high nitrate availability and favorable electrolyte pH resulted in near-complete conversion efficiency and a high yield rate.

In contrast, Zhang et al. reported significantly lower performance with the CoP/CC catalyst in a much lower nitrate concentration electrolyte of 0.005 M $NaNO_3$ and 1 M NaOH, resulting in an ammonia production rate of 0.018 mmol h^{-1} cm^{-2} and a FE of 65 % [62]. The limited nitrate availability in this case reduced the probability of nitrate ions reaching the catalytic centers, slowing down the overall reaction rate. Moreover, under such low nitrate concentrations, the competition between nitrate reduction and other side reactions, such as hydrogen evolution, becomes more prominent. In this environment, limited nitrate ions are accessible to attach to the catalyst surface, leading to fewer productive catalytic cycles. Additionally, the lack of sufficient nitrate ions can lead to more hydrogen evolution as the available protons are reduced, further limiting the electrons available for nitrate reduction.

2.3.3. Coupled reaction systems for enhanced system efficiency

The Zn-NO_3^- battery is an emerging electrochemical system that couples nitrate reduction with energy storage, offering a dual benefit of environmental remediation and energy generation [63–65]. In this system, nitrate ions act as the oxidizing agent in the cathode, where they undergo reduction to ammonia or other nitrogenous products, while zinc is oxidized at the anode. The coupled reactions enable efficient nitrate conversion, and the energy produced can be stored within the battery, enhancing the sustainability of the overall process. For example, Liu et al. built a battery by applying Co_2AlO_4/CC and Zn plate as the cathode and anode, respectively [66]. This battery exhibited an exceptional power density of 3.43 mW cm^{-2} at the *j* of 9 mA cm^{-2}, substantially surpassing the recently reported Pd/TiO_2-based Zn-NO_3^- battery (0.87 mW cm^{-2}). Additionally, Liu et al. utilized $NiCo_2O_4$ as a cathode and Zn plate as the anode to build a Zn-NO_3^- battery to assess the possibility of $NiCo_2O_4$ for operational NH_3 synthesis devices [67]. Remarkably, the battery produced a large NH_3 yield rate of 48.5 μmol h^{-1} cm^{-2} at 12 mA cm^{-2} and demonstrated an impressive FE of 96.1 % at 8 mA cm^{-2}, exceeding recent Pd/TiO_2-Zn-based battery (NH_3 yield: 32.0 μmol h^{-1} cm^{-2}, FE: 81.3 %). Furthermore, Li et al. confirmed the long-term operation stability of Zn-NO_3^- batteries through 8 h of continuous discharging test at 25 mA cm^{-2}, with the FEs (around 88 %) and NH_3 yield (around 110 μmol h^{-1} cm^{-2}).

3. Validation of co active sites and summary of catalyst design strategies

3.1. Identification of co active sites

3.1.1. Co lattice facet

The catalytic properties of Co-based catalysts can be significantly influenced by the exposed lattice facets, as different facets exhibit distinct atomic arrangements that affect the adsorption and activation of reactants [98–100]. Zhu et al. synthesized a series of Co_3O_4 nanostructures with exposed (100), (111), (110), and (112) facets to investigate the influence of crystallographic orientation on electrocatalytic nitrate reduction reaction activity [101]. Among these, Co_3O_4 (111) facet demonstrated the highest activity, achieving an ammonia FE of 99.1 ± 1.8 % and an NH_3 yield rate of 35.2 ± 0.6 mg h^{-1} cm^{-2} at −0.6 V vs. RHE. Both experimental and theoretical analyses revealed a sequential transformation pathway in which the active phases evolved from Co_3O_4 to oxygen-deficient Co_3O_{4-x} with oxygen vacancies (O_v), then to a Co_3O_{4-x}-O_v/$Co(OH)_2$ hybrid, and ultimately to $Co(OH)_2$. This phase evolution occurred across all facets; however, the generation of O_v and $Co(OH)_2$ proceeded most rapidly on the (111) surface. The unique geometric structure of the Co (111) surface promotes efficient adsorption and dissociation of reactant molecules, thereby significantly boosting catalytic activity and overall efficiency. Lu et al. found that as the dominant facet of Co_3O_4 transitioned from (112) to (111), the rate-determining step shifted from $*NO_2 \rightarrow *NO_2H$ to $*NO_3H \rightarrow *NO_2$, reducing the energy barrier to 0.48 eV. This transformation significantly enhanced the hydrogenation of NO_x and NH_x intermediates, leading to an NH_3 yield of 5.73 mg h^{-1} mg_{cat}^{-1} [102].

Although the Co (111) facet shows outstanding NO_3RR performance, other facets can also play a crucial role in catalytic behavior. Zhong et al. revealed that introducing oxygen vacancies on the Co (100) facet facilitated water dissociation and optimized HER intermediate utilization, resulting in a 70 % enhancement in hydrogenation ability [103]. This shift in reaction pathway, from hydrogen evolution to hydrogenation, suggests that the Co (100) facet can be effectively engineered for NO_3RR. Additionally, Lin et al. applied theoretical calculations to explore thermodynamic diagrams of transition metal catalysts for the

NO_3RR [104]. Their findings revealed that the Co (001) surface exhibited ultralow rate-determining free energy change, suggesting superior catalytic activity for both NO_3RR compared to other transition metals.

3.1.2. Co valence

The specific cobalt species present on the catalyst surface have a crucial impact on both catalytic activity and selectivity. The varying oxidation states of cobalt (e.g., Co^0, Co^{2+}, and Co^{3+}) and their corresponding coordination environments can drastically affect the electronic characteristics of the catalyst [105–107]. These differences in oxidation state and coordination geometry can modify the electron density of active sites, thus affecting the adsorption strength of reactant molecules, the binding of intermediates, and the energy barriers for key reaction steps [108]. For instance, Co^{2+} and Co^{3+} species exhibit distinct catalytic behaviors, with Co^{2+} often being more active in certain reactions due to its greater ease in donating electrons. The coexistence of mixed valence states, such as Co^{2+} and Co^{3+}, can also generate redox-active sites that enhance overall catalytic performance [109–112]. In a study by Fu et al., the synergy between Co^{3+} and Co^{2+} in Co_3O_4 for the electrochemical nitrate reduction reaction was investigated using DFT calculations [113]. The energy barrier for adsorbed hydrogen formation (ΔG_{H^*}) was found to be 0.25 eV for Co^{2+}, lower than the 0.37 eV for Co^{3+}, indicating that Co^{2+} requires less energy for *H formation (Fig. 3b). Furthermore, analysis of the d-band center (ε_d) values revealed that Co^{3+} had a stronger interaction with NO_3^-, as its ε_d was closer to the Fermi level (−0.545 eV for Co^{3+} compared to −0.554 eV for Co^{2+}). The study further simulated four Co(II)/Co(III) ratios to optimize the synergy between the two oxidation states, identifying a ratio of 1.33 as the most effective. At this ratio, the lowest ΔG_{H^*} of 0.46 eV was observed, along with the highest ε_d value of −0.554 eV. These results indicated enhanced *H formation and stronger NO_3^- adsorption, demonstrating that the Co (II)/Co(III) ratio of 1.33 provided superior catalytic performance.

3.1.3. Electronic structure

One key advantage of cobalt's electronic structure contributes to its superior catalytic performance in NO_3RR: its favorable d-band center energy (E_d). Carvalho et al. demonstrated that ammonia selectivity tended to increase as the transition metal E_d approached or surpassed the Fermi level (E_F) (Fig. 3c) [114]. This observation can be explained by the d-band model: the antibonding molecular orbital formed between adsorbed *NO and the transition metal surface became increasingly unoccupied as E_d approached and overcame E_F, manifesting as stronger binding (more negative ΔG^*_{NO}) and a preference towards dissociative adsorption ($\Delta G^*_{N+}{}^*_O < G^*_{NO}$). Notably, the E_d value of Co was closely approached E_F, exhibiting exceptionally high selectivity, even when compared to materials with similar E_d values. This was further clarified by DFT calculations that cobalt's high selectivity is due to two key factors: (1) its strong binding affinity for nitrite (NO_2*), which facilitated subsequent reduction, and (2) its promotion of nitric oxide (NO*)

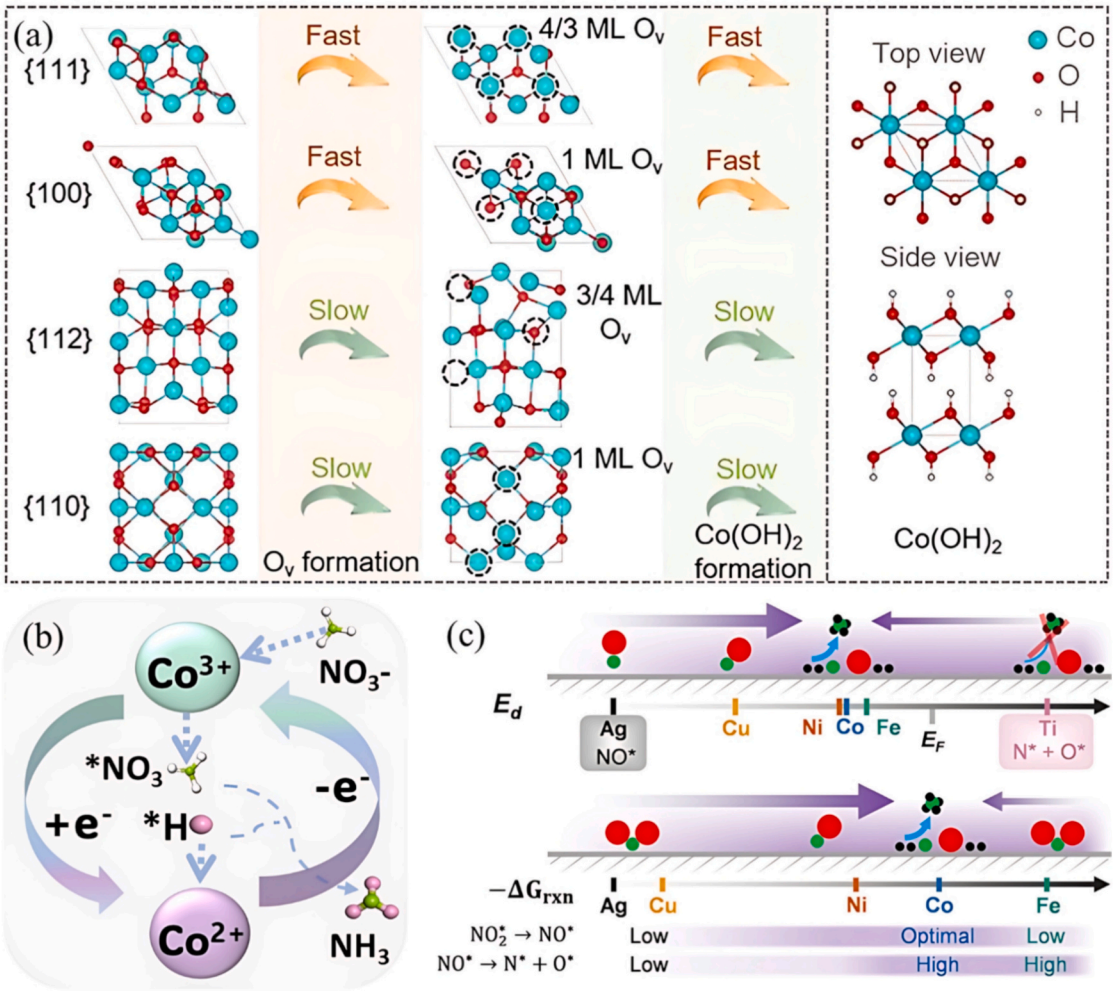

Fig.3. (a) Active component evolution of the Co_3O_4 (111)/(100)/(112)/(110) catalyst during NO_3RR. Reproduced with permission [101]. Copyright 2024, American Chemical Society. (b) Synergy between Co^{2+} and Co^{3+} for NO_3RR. (c) ΔG_{rxn} of nitrite reduction to nitric oxide and ΔG_{rxn}, E_d, and E_F of nitric oxide dissociation on a series of metals. Reproduced with permission [114]. Copyright 2022, American Chemical Society.

dissociation, which induced the targeted conversion of nitrogen adatoms (N*) into ammonia.

Metallic Co facilitates H_2O dissociation, providing the necessary protons for the reaction. However, its electron-rich state often weakens the electrostatic adsorption of NO_3^- and hinders the subsequent formation of $*NH_x$ species. In contrast, oxidized Co species (e.g., $Co^{\delta+}$, Co^+, Co^{2+}, and Co^{3+}) exhibit strong electrostatic interactions with NO_3^-, promoting its adsorption and activation. Unfortunately, these oxidized

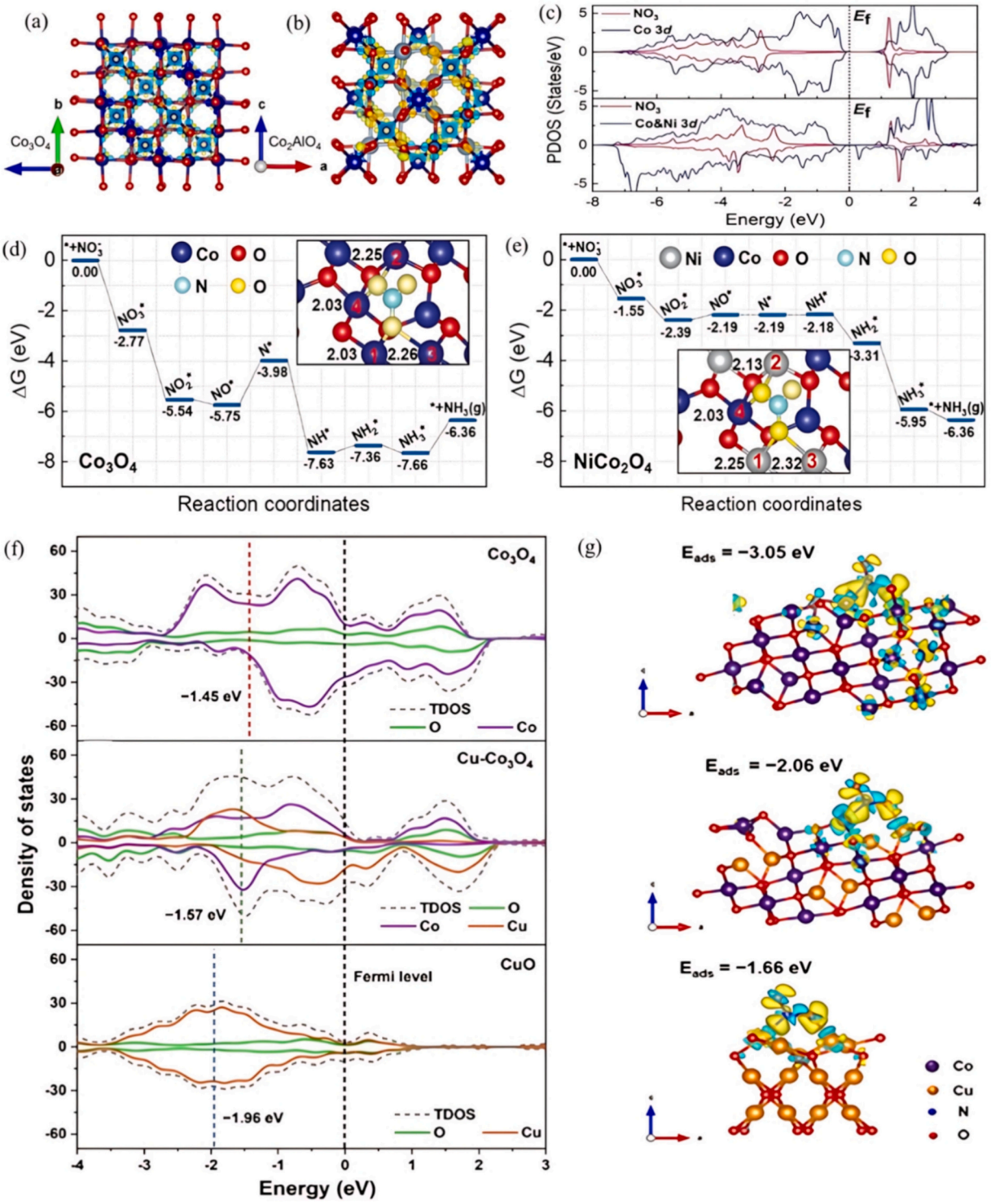

Fig. 4. Differential charge density of (a) Co_3O_4 and (b) Co_2AlO_4, where cyan and yellow isosurfaces represent regions of electron depletion and accumulation, respectively. Reproduced with permission [66]. Copyright 2022, Elsevier. (c) PDOS plots for NO_3^- adsorption on Co_3O_4 (311) and $NiCo_2O_4$ (311) surfaces, shown in the upper and lower panels, respectively. The E_f is marked by the vertical dashed line. Free energy plots for the NO_3RR on the (d) Co_3O_4 (311) and (e) $NiCo_2O_4$ (311) surfaces. Inset figures illustrate the local structures for NO_3^- adsorption, with the bond lengths between O and Ni/Co atoms presented in black values. Reproduced with permission [67]. Copyright 2022, John Wiley and Sons. (f) DOS of Co_3O_4, Cu-Co_3O_4, and CuO. (g) Variation in charge density for $*NO_2$ on Co_3O_4, Cu-Co_3O_4, and CuO, where the yellow and cyan electron clouds represent charge accumulation and depletion, respectively. Reproduced with permission [71]. Copyright 2022, American Chemical Society. (For interpretation of the references to colour in this figure legend, the reader is referred to the web version of this article.)

Co compounds generally have a limited capacity for H_2O dissociation, leading to insufficient proton supply, which negatively impacts the hydrogenation process of *NH_x species. Therefore, rational catalyst design strategies should be employed to finely tune the electronic structure of Co/Co oxides, optimizing their ability to concurrently adsorb and activate hydrogen atoms, nitrate ions, and nitrogen-containing intermediates [115,116].

3.2. Strategic approaches to catalyst design

3.2.1. Transition metal modification

The transition metal modification of cobalt-based catalysts represents a powerful strategy to enhance their catalytic performance, selectivity, and stability [117]. One prominent approach is the formation of spinel oxides, where cobalt is integrated with other transition metals (such as manganese, nickel, or iron) into a spinel oxide structure. Spinel oxides, with their robust crystalline framework, offer excellent stability and electronic conductivity, while providing a high density of active sites [118,119]. The synergistic interactions between cobalt and other metal cations in the spinel structure can fine-tune the electronic structure, optimize active sites, and improve the catalyst's resistance to deactivation. For example, Deng et al. revealed that Co ions in Co_2AlO_4 exhibited a further depletion of charge, resulting in a reduced electron charge density (evident in the cyan region) relative to Co_3O_4 [66]. This charge depletion led to an increase in the valence state of Co ions in Co_2AlO_4, strengthening the covalent interactions between bonding atoms and enhancing the structural stability (Fig. 4a and b). Liu et al. showed that the electronic states of overlap more extensively with the 3d orbitals of adjacent Co atoms on Co_3O_4 (311) compared to the overlap with both Co and Ni atoms on $NiCo_2O_4$ (311), indicating robust NO_3^- binding on Co_3O_4 (311) (Fig. 4c) [67]. This aligns with the observation that exceptional catalysis exhibited by $NiCo_2O_4$ arised from its moderate adsorption of NO_3^- and the optimized adsorption energy (NO*-N*), facilitated by nickel in its crystal structure (Fig. 4d and e).

Additionally, a trace amount doping of a foreign transition metal into the cobalt matrix, altering its electronic configuration and the d-band center. These modifications enable the fine control of reaction pathways and the stabilization of active intermediates, enhancing its activity and selectivity. For example, Niu et al. manifested that the d-band center energy level of Cu-Co_3O_4 (−1.57 eV) is between Co_3O_4 (−1.45 eV) and CuO (−1.96 eV) through the density of states (DOS) (Fig. 4f) [71]. The adsorption energy of *NO_2 on Cu-Co_3O_4 is between that of Co_3O_4 and CuO, indicating an optimized adsorption capacity for NO_3RR intermediates. Differential charge density maps confirmed that Cu species improve charge redistribution, enhancing the catalytic performance of Co_3O_4 (Fig. 4g).

3.2.2. Non-metal heteroatom modification

In addition to transition metal modification, non-metal heteroatom (e.g., P, S, and B) modification, particularly with phosphorus (P), has also been proven effective in improving NO_3RR performance [120–122]. The modification of non-metal heteroatom on cobalt materials introduces new active sites, enhances electron transfer, and increases the stability of the catalyst under electrochemical conditions [77–79,123]. For example, Gao et al. synthesized P-doped Co_3O_4 for nitrate reduction and found that P doping enhanced the electrochemically active surface area while reducing the interface impedance of Co_3O_4 [124]. The Co-P@NF catalyst synthesized by Fan et al. demonstrated exceptional long-term stability, sustaining an NH_3 FE of over 90 % and a current density of 799 mA cm^{-2} after 82 h of electrolysis [125]. Li et al. revealed that octahedral CoS_2 (CoS_2 OC) can effectively convert NO_3^- to NH_3 with a high performance (NH_3 yield rate: 10.6 ± 0.4 mg h^{-1} cm^{-2}, FE: 96 ± 1.5 %) [126]. Xie et al. highlighted the critical role of an in-situ derived Co_2B nanosheet array supported on a Co_3O_4/Ti, which exhibited a maximum FE of 97.0 % at −0.70 V vs. RHE and a remarkable NH_3 yield of 8.57 mg h^{-1} cm^{-2} at −1.0 V vs. RHE, with durability for stable NO_3^- to NH_3 conversion over eight recycling tests and 12 h of electrolysis [127].

The modification of P could modulate the electron configuration of the catalyst to enhance the nitrate ions interaction with the catalyst surface, thereby facilitating the NO_3RR performance. Ye et al. disclosed that the excited electrons in Co 4p orbital were transported to the O 2p orbitals and delivered into the p* orbitals of NO_3^- through the Co-O-N covalent bond, causing destabilization and reduction of the adsorbed NO_3^- due to the elongation of Co—P bond (Fig. 5a) [61]. Additionally, in the nitrate reduction reaction, the presence of phosphorus helps to stabilize the intermediate species and reduce the energy barriers associated with the reaction steps, which is essential for promoting the nitrate reduction kinetics. Fan et al. found that the rate-determining step (RDS) for CoP was the conversion of NO* to HNO*, with a lower ΔG uphill of 1.57 eV, whereas for Co, the RDS was the conversion of NO_2* to HNO_2*, requiring a significantly higher ΔG of 3.09 eV (Fig. 5b) [56]. Besides, the entire reaction pathway on the CoP surface was much smoother compared to that on Co. Gao et al. further highlighted the critical role of P in regulating *H atoms to achieve high selectivity towards ammonia production [124]. Specifically, P doping not only facilitated *H formation through water dissociation but also strengthened *H adsorption on the catalyst surface, effectively suppressing H_2 formation (Fig. 5c). Zhao et al. also demonstrated that an optimized amount of CoS_2 could balance the adsorption of *H and NO_3^- on the catalyst surface, thereby mitigating excessive HER and enhancing NO_3RR performance [128]. Similarly, Zhang et al. emphasized that the introduction of Co—B into the catalyst structure could effectively suppresses the competitive HER by facilitating controlled *H generation through water dissociation [129]. This regulated provision of *H precisely promotes the hydrogenation step in the NO_3RR, ensuring a more selective and efficient nitrate-to-ammonia conversion.

3.2.3. Defect engineering

Defect engineering has emerged as a pivotal strategy in the synthesis of Co-based catalysts for the nitrate electroreduction process. This approach involves the deliberate introduction of structural imperfections into the lattice of catalysts, such as vacancies, dislocations, and edge sites [130,131]. These defects serve as a critical factor in promoting the reaction efficiency by modifying the electronic structure, maximizing active site availability, and improving the sorption and activation of nitrate molecules. Traditionally, the controlled introduction of defects could be achieved through synthesis methods such as high-energy ball milling [132], chemical vapor deposition [133], thermal annealing [134] and hydrothermal synthesis [135]. Notably, Chen et al. developed a novel plasma-engraving method to enhance surface oxygen vacancy on Co_3O_4, increasing it from 24 % to 57 % [136].

To leverage the benefits of defects, their identification and characterization through advanced techniques are essential. For example, the increased peak intensity in Raman spectroscopy of v_{Co}-Co_3O_4 indicated the presence of cobalt vacancies on Co_3O_4, which were further verified by the stronger electron paramagnetic resonance (EPR) spectra signal compared to the pristine Co_3O_4 (Fig. 6a) [137]. Additionally, Co K-edge X-ray Absorption Near Edge Structure (XANES) and Extended X-Ray Absorption Fine Structure (EXAFS) spectroscopy can offer deeper insights into how surface defects alter the coordination environment of catalysts [136]. A flatter and wider main edge peak was found in v_o-Co_3O_4 compared to Co_3O_4, attributed to abundant oxygen vacancies resulting from low molecular symmetry (Fig. 6b). The first shell coordination fitting (Co—O at 1.5 Å) indicated that v_o-Co_3O_4 possessed more coordination numbers than Co_3O_4 (Fig. 6c). Moreover, the electron transfer characteristics of catalysts could also be impacted by surface defects, as indicated by the projected density of states (PDOS) and in situ Co X-ray absorption (XAS) spectroscopy. In contrast to pure CoO_x sample, O_v-CoO_x exhibited a new peak near the Fermi level as shown in PDOS, leading to an increased electron density and improved electrical conductivity (Fig. 6d) [138]. The study by Chen et al. provided direct evidence of electron transfer induced by oxygen vacancy [136]. In v_o-

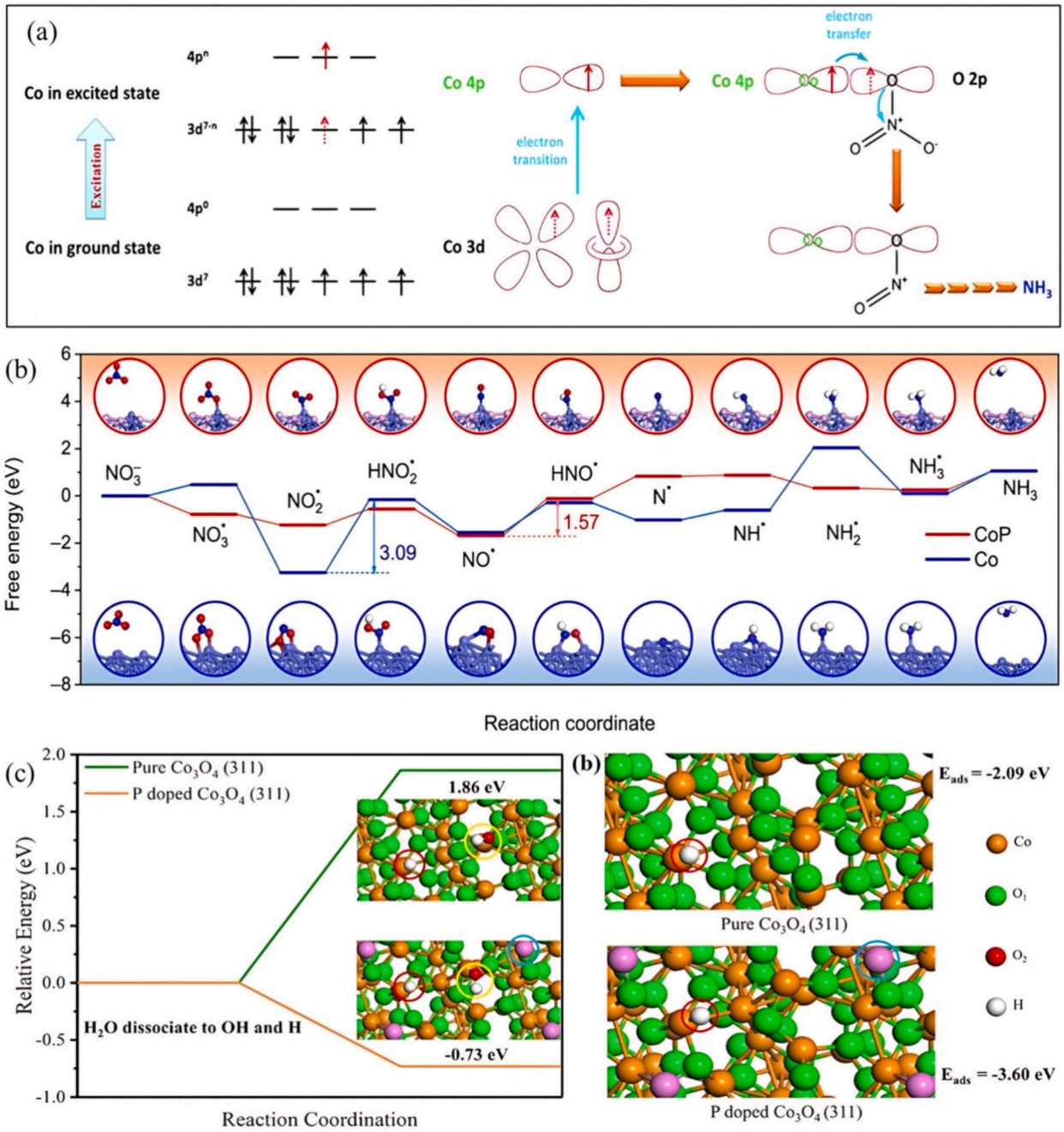

Fig.5. (a) Electron interaction between CoP and reactants. Reproduced with permission [61]. Copyright 2022, Royal Society of Chemistry. (b) NO_3RR processes on CoP (211) and Co (111) surfaces [56]. (c) The relative energy for H formation from H_2O dissociation and adsorption energy for H atom on pure Co_3O_4 (311) and P doped Co_3O_4 (311), respectively. Reproduced with permission [124]. Copyright 2020, Elsevier.

Co_3O_4, oxygen vacancies left two electrons in neighboring cobalt ions, leading to the conversion of Co^{3+} (Oh) to Co^{2+} (Oh), serving as electronic donors to contribute to charge the π* orbital of nitrate (Fig. 6e–g).

3.2.4. *Single atom surface engineering*

Single atom catalysts (SACs), first proposed in 2011, are a class of heterogeneous catalysts where individual metal atoms are dispersed and stabilized on a support material. Support is considered a critical part of the SACs system, playing an essential role in enhancing the activity of metal atom centers and the adsorption of reactants [139–141]. An exceptional support often demonstrates a modifiable coordination environment and outstanding interactions with individual metal atoms, leading to an optimized metal atom-support combination and a reduction in the free surface energy of SACs. Carbon-based materials are extensively employed as the substrate in various electrocatalysts due to their advantages, including modifiable shapes, strong electrical conductivity, and excellent thermal resistance. For example, Kain et al. developed CoO functionalized on graphene for the targeted nitrate-to-ammonia reduction, achieving a nearly 100 % NH_3 FE and a high NH_3 yield of 25.63 mol g^{-1} h^{-1} [97]. Furthermore, catalytic performance can be enhanced by adjusting electronegativity through the introduction of heteroatom substituting N in the nitrogen-doped carbon (NC) support. For instance, Li et al. synthesized Co single-atom catalysts (Co-SACs) stabilized on an N-doped carbon, along with P introduction to enlarge defects and create extra sites for immobilizing single metal atoms, resulting in superior metal-support interactions (SMSIs) and CoP1N3

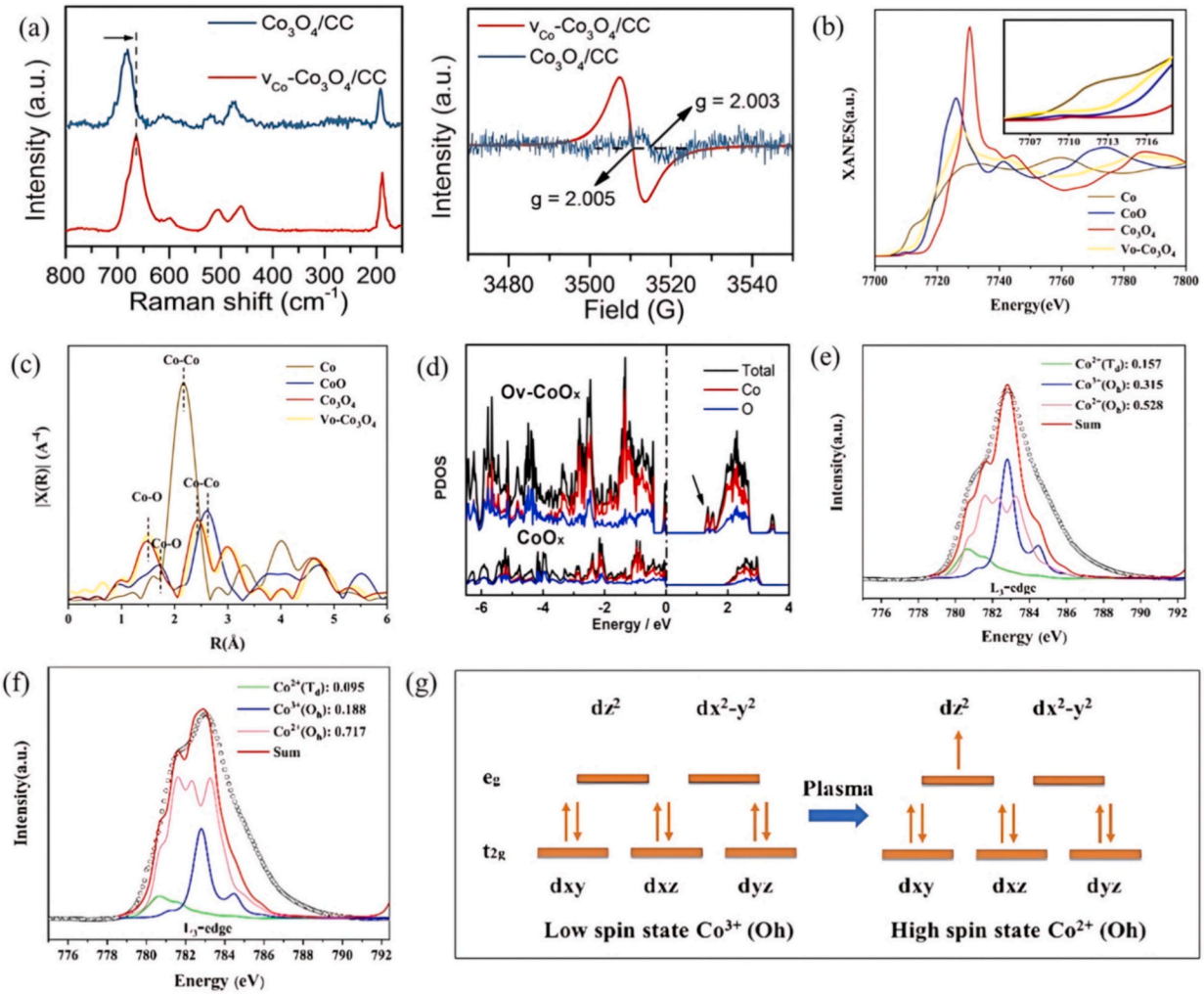

Fig.6. (a) Raman and EPR spectra in the Co 2p regions for Co_3O_4/CC and v_{Co}-Co_3O_4/CC. Reproduced with permission [137]. Copyright 2022, American Chemical Society. (b) Normalized Co K-edge XANES spectra (c) Co K-edge EXAFS spectra in R space of Vo-Co_3O_4 and Co_3O_4. Reproduced with permission [136]. Copyright 2022, Elsevier. (d) PDOS of O_v-CoO_x and pure CoO_x. Reproduced with permission [138]. Copyright 2019, Elsevier. CTM calculations are used to model experimental XAS spectra of (e) nanoporous Co_3O_4 and (f) nanoporous v_o-Co_3O_4, along with (g) the schematic diagram of charge the spin state of Co^{3+} (Oh) and Co^{2+} (Oh). Reproduced with permission [136]. Copyright 2022, Elsevier.

coordination structures (Figs. 7a–b) [93]. The SMSI effect adjusted the immediate environment and Co center electron configuration and enhanced the uniformity and resilience of single Co atoms, thereby promoting NH_4^+ generation (Fig. 7c).

In the case of cobalt-based SACs derived from metal-organic frames (MOFs), the synthesis typically involves the pyrolysis of cobalt-containing MOFs under controlled conditions to create isolated cobalt atoms dispersed on a carbonaceous matrix. During the pyrolysis process, the calcination temperature serves as an important role to determining the structure and performance of SACs [60]. MOF-derived carbon material supports commonly exhibit micro- or mesopores with pore sizes below 5 nm, restricting the direct contact of active metal sites with electrolytes, especially at high metal loadings. To address this issue, three-dimensional (3D) structures with extensive internal void spaces and interlinking pathways have shown the potential to enrich the exposure active sites and facilitate multiple pathways for electron transfer and electrolyte dispersion. For instance, a 3D mesopore-rich SACs (MR *Co*-NC) was synthesized by employing polystyrene (PS) as sacrificial templates, which was decomposed during pyrolysis, leaving behind a highly porous metal-N-C network (Fig. 7d) [82]. SEM images revealed that MR Co-NC, with a hexahedron morphology and 3D interconnected framework, enhanced Co site dispersion compared to Co-NC without a PS template. The hierarchically mesoporous structure, confirmed by a higher BET surface area of 273.74 m^2 g^{-1}, results in improved FE and NH_3 yields.

3.2.5. *Heterostructure engineering*

In the case of NO_3RR, especially under neutral conditions, heterostructures have developed as a prospective pathway for improving the electrochemical performance of Co-based catalysts. By leveraging the distinct electronic structures of the components, heterojunction interfaces can significantly enhance catalytic activity through the induction of an intrinsic electric field [142,143]. This interaction modulates the electronic structure to optimize the surface adsorption energies of reaction species, ultimately enhancing the selectivity and activity of the catalyst. Notably, incorporating n-type or p-type semiconductors can create Mott-Schottky heterostructures, inducing the Mott-Schottky effect. For example, Yu et al. incorporated p-type semiconductor CoO with Co to form a heterostructured Co/CoO nanosheet for nitrate reduction reaction [144]. In the Co/CoO heterostructure, the lower Fermi level of the p-type CoO semiconductor accepted electrons from metallic Co until equilibrium was reached, creating band bending and Schottky barriers due to electron transfer (Fig. 8a). The resulting Co/CoO NSAs have a balanced work function of 5.68 eV and an E_V position of −6.49 eV, slightly higher than that of CoO alone, confirming the presence of Schottky contacts (Fig. 8b). The last step of NH_2* to NH_3 was more

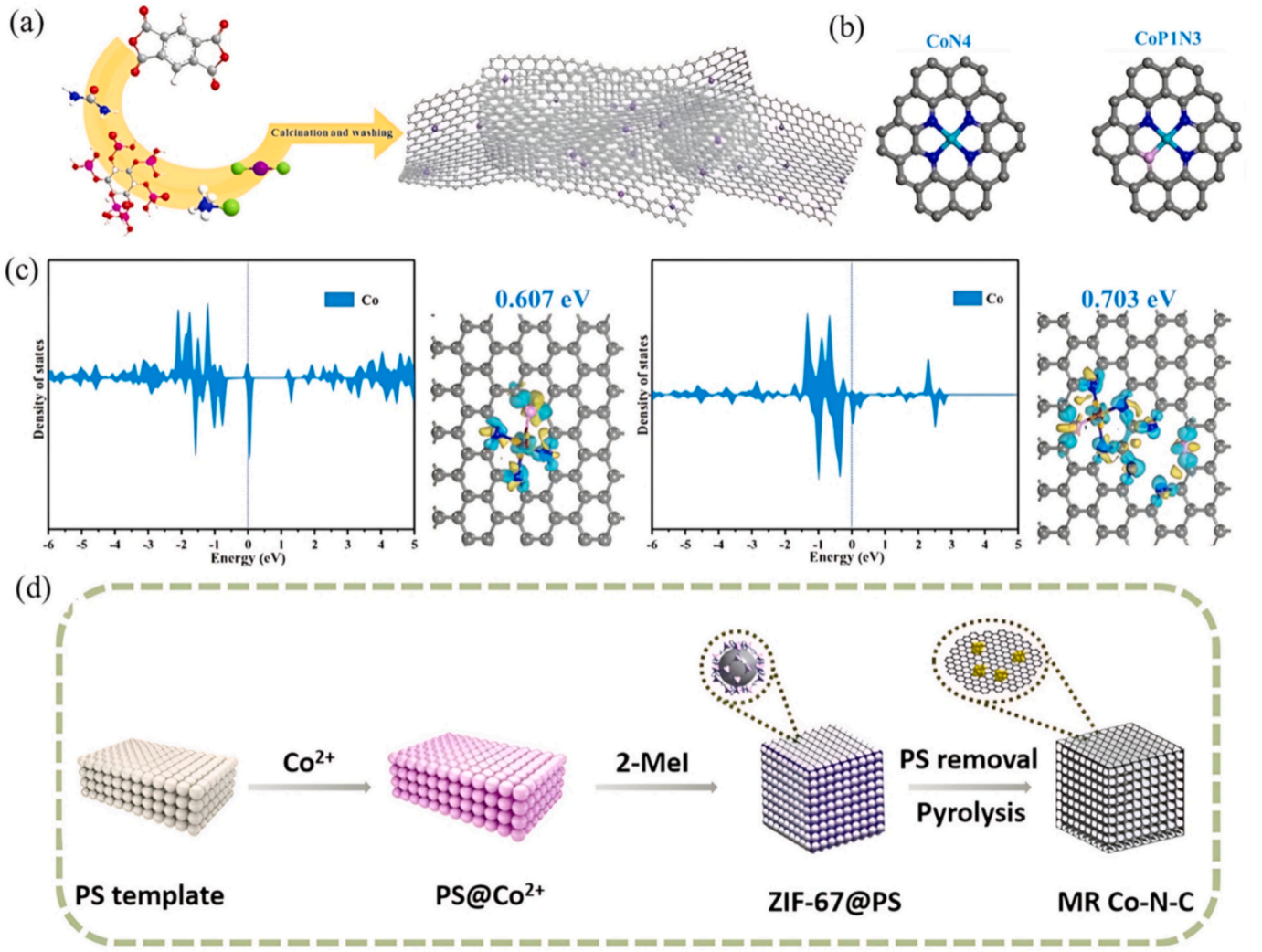

Fig.7. (a) Depiction of the synthesis process for Co SACs. (b) Fitted configuration models for CoN4 and CoP1N3 in Co-CN and Co-CNP. (c) PDOS for the CoP1N3 center and its interaction with P1N3 defects; Charge density differences in CoP1N3 sites and the interaction between CoP1N3 sites and P1N3 defect. The gray, blue, pink, and red spheres represent C, N, P, and Co atoms, respectively, while the yellow and cyan regions indicate areas of electron accumulation and depletion, respectively. a.u., arbitrary units [93]. (d) Illustrative diagram of the synthesis steps of MR Co-NC. Reproduced with permission [82]. Copyright 2023, Elsevier. (For interpretation of the references to colour in this figure legend, the reader is referred to the web version of this article.)

favorable for Co/CoO NSAs, with an energy discharge of 0.41 eV, compared to Co NSAs, which showed an energy rise of 0.07 eV (Fig. 8c). In addition, the Co/CoO NSAs exhibited a higher energy barrier for H_2 and other byproducts (NO, N_2, N_2H_4 and N_2O) formation compared to Co NSAs (Fig. 8d), indicating a suppressive effect on H_2 production. This increased energy requirement for by-product formation suggests that Co/CoO NSAs provide a more selective pathway for nitrate reduction to ammonia, enhancing overall catalytic selectivity. Fan and co-authors combined n-type TiO_2 with Co to create a Co@TiO_2 heterostructure with a Schottky interface, enhancing nitrate reduction to ammonia in a neutral solution [84]. It was proved that electrons transferred from Co to TiO_2, creating electron-depleted zones on the Co surface and exhaustion areas at the interface. The Schottky junction of Co@TiO_2 can largely increase electron transport capability, accelerate NO_3^- adsorption, facilitate the rate-limiting step, and improve catalytic target selectivity, thereby resulting in superior NO_3RR performance.

3.2.6. *In-situ reconstruction of catalysts*

In-situ reconstruction refers to the physical or chemical structural changes that occur in electrocatalysts during electrochemical process, including surface morphology adjustments, crystal facet reorganization, and oxidation state transformations [145–147]. For example, Ru-doped Co metal nanosheets underwent in-situ reconstruction into Ru|β-Co$(OH)_2$ heterostructures, maintaining their original nanosheet-like morphology while also forming new, orderly stacked nanosheets during the NO_3RR under alkaline conditions (Fig. 9a). This transformation was evidenced by a biphasic structure comprising hexagonal Ru and Co$(OH)_2$, as confirmed by selected area electron diffraction (SAED) patterns [148,149]. Structural reconstruction typically occurs under external influences such as the reaction medium, potential, or temperature. Ion leaching-the selective dissolution of specific elements (e.g., P, W, and Mo) and element doping (e.g., Ni) can further enhance this process by inducing defects, generating new active sites, and promoting phase transitions [150–153]. For instance, upon exposure to KOH solution, the P element on the surface of CoP rapidly dissolved, resulting in the formation of a core@shell CoP@Co$(OH)_2$ structure. This structure can further be electrochemically reduced to CoP@Co through a pre-reduction process prior to the nitrate reduction reaction (NO_3RR) [153].

The reconstructed structure in the catalytic process can play a crucial role in enhancing catalytic performance through multiple mechanisms. It may regulate the electronic configuration of the original metal, optimizing charge distribution and modulating the adsorption energy of key

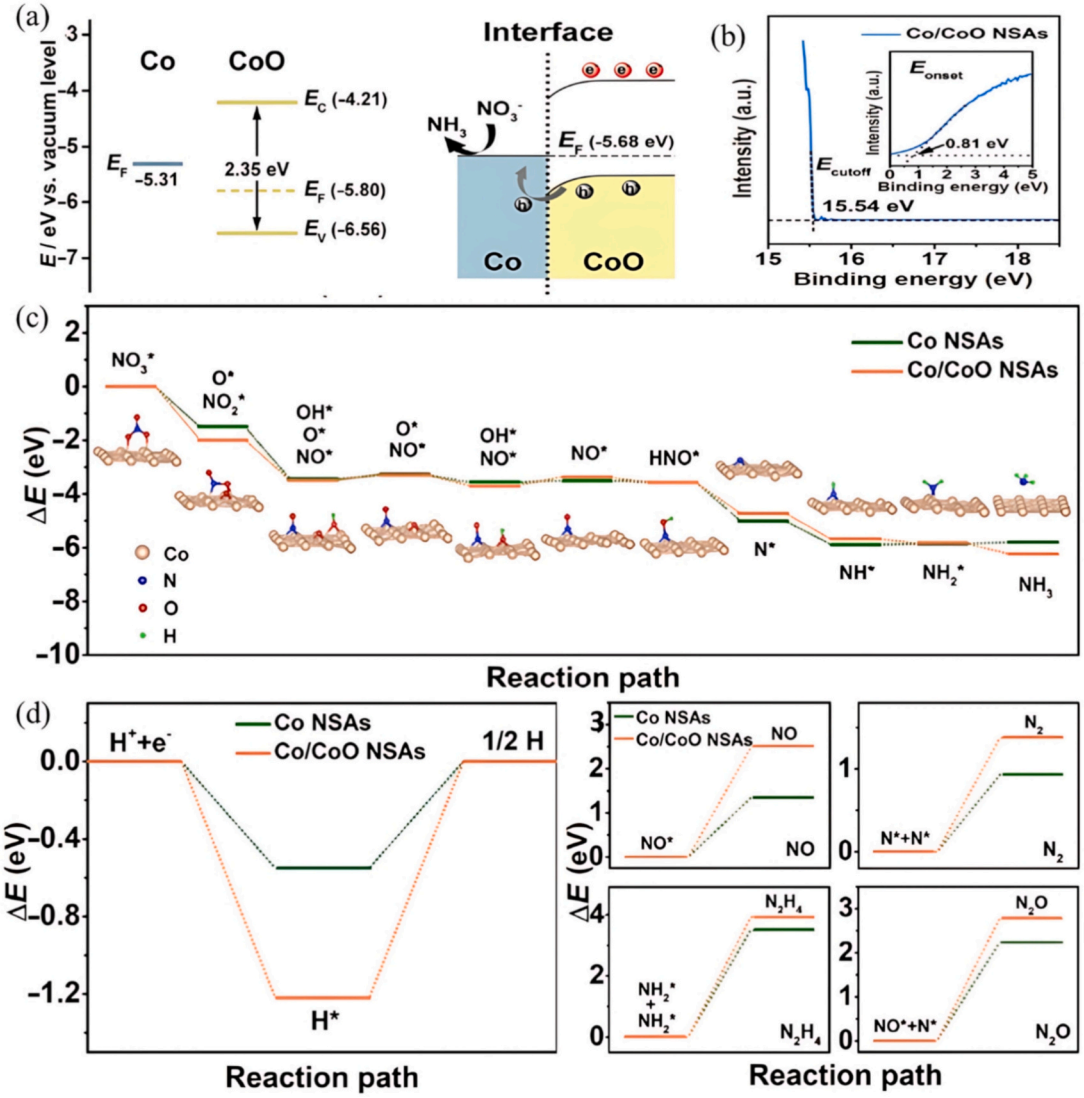

Fig.8. (a) Schematic representation of the energy bands for Co metal and CoO p-type semiconductor (E_F: Fermi level; E_V: valence band energy; E_C: conduction band energy), and an illustration of electron transfer in Co/CoO NSAs. (b) UPS spectra for Co/CoO NSAs in the cutoff energy region (inset illustrating the onset energy region). (c) DFT-calculated free energy diagram. (d) The computed reaction energy difference of H_2 generation on Co and Co/CoO NSAs and the computed reaction energy difference of the generation of NO, N_2, N_2H_4 and N_2O on Co and Co/CoO NSAs. Reproduced with permission [144]. Copyright 2020, Springer Nature.

reaction intermediates. For example, in the evolved Ru/β-$Co(OH)_2$ heterostructure, the interfacial Ru atoms exhibited a distinct electron-deficient state, while the interfacial Co atoms displayed an electron-enriched state (Fig. 9b). The interfacial electron-deficient Ru active sites weakened the d-p orbital hybridization with *NH_3 intermediates and thus accelerated the final *NH_3 desorption, resulting in an improved NO_3RR activity (Fig. 9c–d). Additionally, the reconstructed phase can introduce new active sites, either generating defects such as oxygen vacancies, or forming heterostructures, which may directly participate in the catalytic reaction, improving reaction kinetics and selectivity. Gong et al. investigated the synergistic role of the $CoWO_4$/CoOOH heterostructure in catalysis, which evolved from $CoWO_4$. In this system, CoOOH enhanced the adsorption of N-containing intermediates, while $CoWO_4$ supplied *H for their hydrogenation (Fig. 9e). DFT calculations further revealed that the $CoWO_4$/CoOOH heterostructure facilitated NH_3 desorption, improving the overall reaction efficiency (Fig. 9f).

3.2.7. *Analysis of current catalyst design strategies*

Above catalyst design strategies could fine-tune the electronic structure, regulate active sites, and improve reaction kinetics. Each approach offers unique advantages, such as enhanced electron transfer, optimized adsorption energy, or increased catalytic synergy, but also presents challenges such as phase segregation, structural instability, or fabrication complexity [154,155]. A comparative analysis of these methods provides insight into their respective strengths and limitations, guiding the rational design of advanced cobalt-based catalysts for efficient electrochemical nitrate-to-ammonia conversion (Fig. 10). Transition metal incorporation (e.g., Fe, Ni, and Cu) tunes the electronic structure by altering the d-band center, enhancing electron transfer, and improving catalytic activity and stability, although phase segregation and metal dissolution may occur. Heteroatom doping (e.g., P, S, and B) redistributes charge density and adjusts local electronic states to improve conductivity and selectivity, but precise control over doping sites remains challenging. Vacancy engineering (e.g., oxygen) or lattice distortion modifies local electron states, optimizes adsorption energy, and enhances active site exposure, yet may lead to structural instability. Single-atom isolation on conductive supports or stabilization with ligands maximizes atomic utilization and adjusts electronic properties for high catalytic efficiency and tunable selectivity, though synthesis and stability present challenges. Interface engineering between Co-based

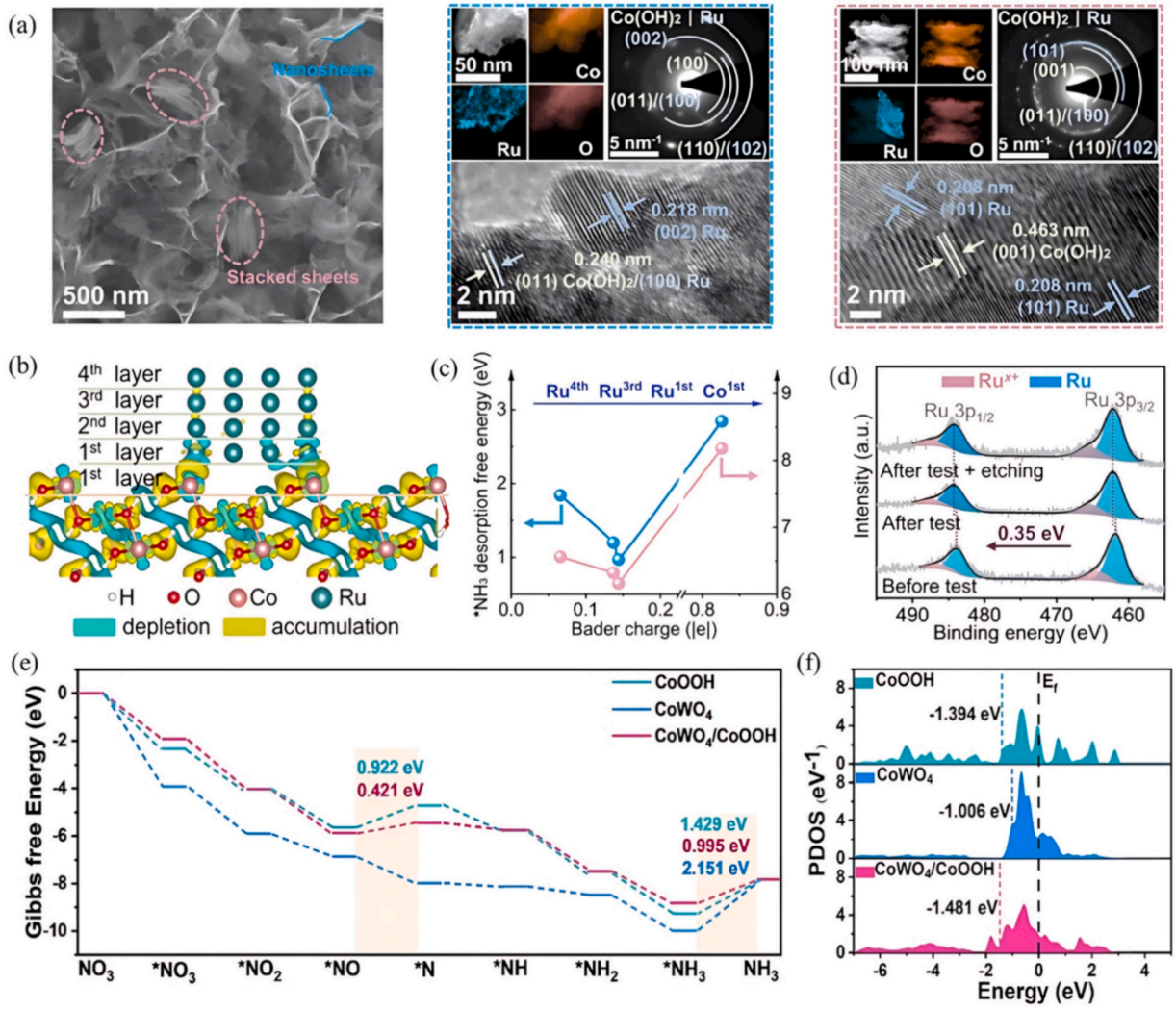

Fig.9. (a) Structural characterization of the RuCo catalyst after the NO_3RR. SEM image, HAADF-STEM images and the corresponding elemental maps, SAED patterns and HRTEM images of "original" nanosheets and newly formed stacked nanosheets. (b) A differential charge density plot. The yellow and cyan contours represent the electron accumulation and depletion, respectively. (c) Relation among Bader charge, $*NH_3$ desorption free energy and d-p orbital hybridization ability of the metal-$*NH_3$ models. (d) Ru 3p XPS spectra. Reproduced with permission [148]. Copyright 2023, Royal Society of Chemistry. (e) Gibbs free energy diagram of various intermediates produced during NO_3RR over $CoWO_4$, CoOOH and $CoWO_4$/CoOOH. (f) PDOS of NO_3^- over $CoWO_4$, CoOOH and $CoWO_4$/CoOOH. Reproduced with permission [152]. Copyright 2025, Elsevier. (For interpretation of the references to colour in this figure legend, the reader is referred to the web version of this article.)

materials and other functional components enhances electronic interactions and catalytic synergy, despite the fabrication complexity. Lastly, dynamic structural transformation enables in situ electronic state evolution for optimized active sites and self-adaptive behavior yet is difficult to control and characterize dynamically.

4. Challenges and perspectives

Despite significant advancements in Co-based catalysts for electrocatalytic nitrate reduction reaction, several challenges remain that hinder their widespread application and optimal performance. One major challenge is enhancing system output, as traditional NO_3RR systems rely on energy-intensive anodic reactions like the oxygen evolution reaction (OER), which are less cost-effective. Additionally, the multistep nature of NO_3RR—comprising deoxygenation, hydrogenation, and intermediate regulation—makes it difficult for single-component catalysts to maintain both high activity and NH_3 selectivity. Real wastewater conditions further complicate practical implementation, as the dilute and impure nitrate streams hinder reaction efficiency and raise challenges for industrial-scale product recovery and system integration. Building on these challenges, key areas for future perspectives in Co-based NO_3RR are briefly summarized below:

4.1. Exploring bifunctional co-based catalysts for enhanced overall system output

Efforts to optimize NO_3RR systems have emphasized coupling nitrate reduction with alternative anodic reactions to enhance system output while generating valuable co-products, such as containment removal, organic oxidation and plastic waste upgrading, this integrated approach not only drives the nitrate reduction process but also generates valuable co-products (Fig. 11a) [156–158]. For example, Li et al. constructed electrocatalytic denitrification process associated with glycerol oxidation system, achieving significantly increased ammonia generation (15.2 mg h^{-1} cm^{-2}) along with value-enhanced formate (111.4 mg h^{-1} cm^{-2}) at 1.8 V cell voltage through CoP bifunctional catalyst (Fig. 11b) [159]. Initial techno-economic analysis confirmed the financial viability of the integrated system. Reducing the operating voltage in this system

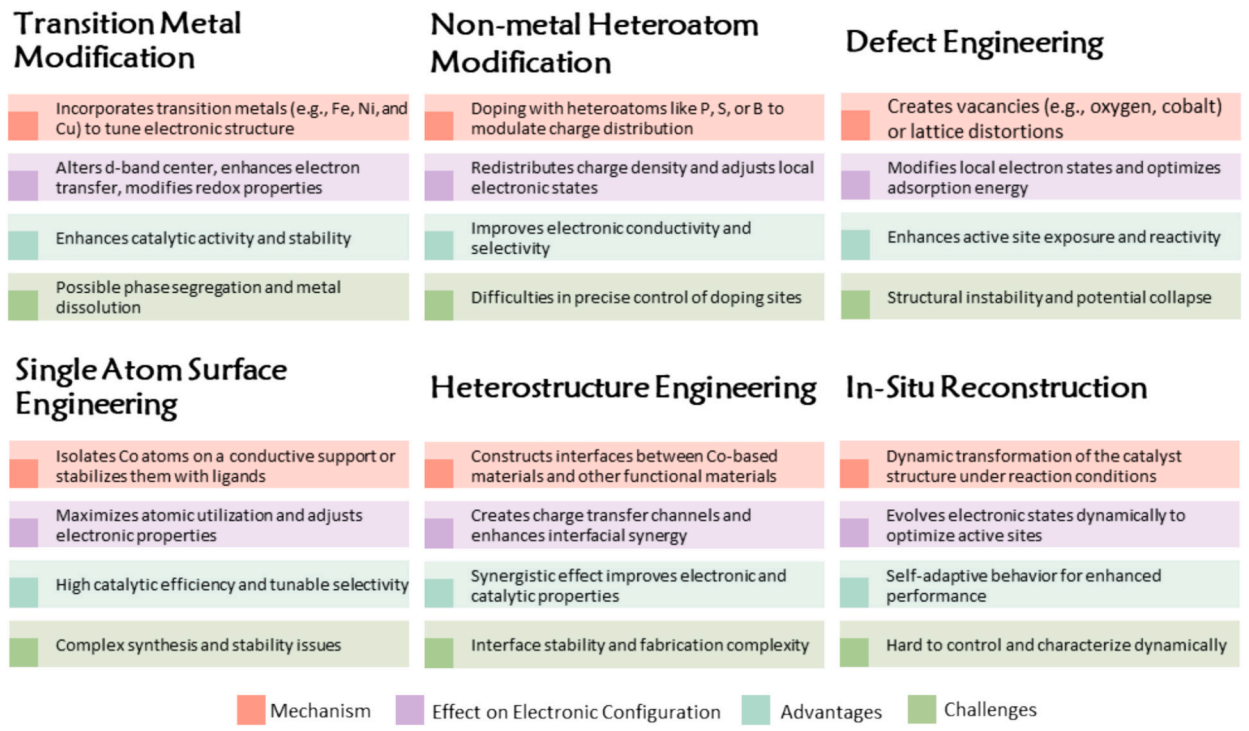

Fig. 10. Comparative analysis of catalyst design strategies.

saved approximately 1400 kWh and $348 per ton of NH_3 produced. Additionally, formic acid ($1200 ton^{-1}) generated at the anode boosted the system's economic value from $2629 ton^{-1} NH_3 (with NO_3RR//OER) to $1217 ton^{-1} NH_3. Further, formic acid can be converted to potassium diformate (KDF), a valuable animal growth promoter ($2500 ton^{-1}), increasing profitability to $4474 ton^{-1} NH_3.

NO_3^--mediated electrosynthesis refers to an electrochemical process that utilizes nitrate ions as a key reactant to synthesize valuable chemical products. This approach typically involves the reduction of nitrate ions, often paired with other reduction reactions to produce compounds like urea, or other nitrogen-containing chemicals. Traditional methods for urea synthesis are energy-intensive, as they typically require ammonia from the Haber-Bosch process and CO_2 fixation under high pressures. An excellent alternative of urea electrosynthesis involves coupling nitrate reduction with CO_2 reduction, avoiding the reliance on conventional nitrogen sources [160]. Outstanding electrocatalytic performance for urea synthesis has been demonstrated from co-reduction of CO_2 and NO_3^- through bifunctional Co single atom catalyst, achieving a significant urea production rate of 2704.2 ± 183.9 mg h^{-1} mg_{cat}^{-1} and a FE of 31.4 ± 2.1 % at −1.5 V vs. RHE [161].

4.2. *Regulating co-involved NO_3RR pathway for improved NH_3 selectivity*

Ensuring high selectivity in ammonia synthesis requires precise control of intermediate steps to prevent undesired side reactions. Relay/tandem catalysis has emerged as a pivotal strategy to address these challenges. By integrating multiple catalytic components or sites, each tailored for a particular step in the reaction pathway, relay catalysis enables more effective management of reaction intermediates. Co-based catalysts exhibit strong reactivity towards the specific reaction step of NO_2^- to NH_3. By integrating Co-based phases with catalytic phases (e.g., Cu), which demonstrate targeted activity for the NO_3^- to NO_2^- conversion, rapid reaction kinetics and high NH_3 selectivity can be effectively achieved. For example, He et al. proposed a rational catalyst design strategy that involved the linear assembly of sub-5 nm Cu/Co nanophases into sub-20 nm thick nanoribbon [162]. The theoretical and experimental studies revealed that the synergistic integration of enhanced NO_3^- adsorption at binary phase boundaries and tandem NO_3^--to-NH_3 reaction in sub-5 nm distance offered a reliable path to achieve high-efficiency NH_3 production (Fig. 11c). Additionally, He et al. also revealed that core-shell Cu/CuO_x and Co/CoO phases, derived from electrochemical transformation of Cu—Co binary sulfides exhibited tandem catalytic performance towards NO_3RR (Fig. 11d) [83]. Specifically, the inner Cu/CuO_x phases preferentially catalyzed NO_3^- reduction to NO_2^-, which was rapidly reduced to NH_3 at the nearby Co/CoO shell. Liu et al. designed a tandem electrocatalyst that merged Cu single atoms with Co_3O_4 nanosheets to promote the electroreduction of NO_3^- to NH_3 [163]. It was revealed that NO_3^- binded more strongly to CuN_4 than Co_3O_4, but $*NO_2$ tended to desorb from CuN_4, leading to NO_2^- accumulation. Meanwhile, Co_3O_4 favored NO_2^- adsorption through stable bonding, making it more effective at reducing NO_2^- to NH_3.

The hydrogen evolution reaction poses a significant competitive challenge to the nitrate reduction reaction. The key to regulating active hydrogen species (*H) lies in promoting active hydrogen generation while suppressing the recombination of hydrogen atoms into hydrogen. For example, in a two-dimensional mesoporous cobalt-copper (meso-CoCu) nanoplate electrocatalyst system, *H radicals generated from water splitting on Co sites transferred to adjacent Cu sites, where they stabilized within confined mesopores (Fig. 11e) [164]. This stabilization kinetically enhanced the hydrogenation of nitrogen intermediates, significantly promoting the NO_3RR and NH_3 selectivity. Additionally, Liang et al. also demonstrated that a Mn-doped $Co(OH)_2$ effectively dissociated H_2O molecules while inhibiting the recombination of H*, attributed to the increased interatomic spacing induced by Mn doping [165].

4.3. *Developing advanced co-based catalysts for optimized NO_3RR performance*

Doping concentration-gradient metals into Co electrocatalysts, with optimized structural and compositional profiles, offer the potential to adapt to varying nitrate concentrations and impurity levels, maintaining activity and selectivity across diverse conditions. Chen et al. developed a concentration-various electrocatalyst composed of Ru atoms in Co

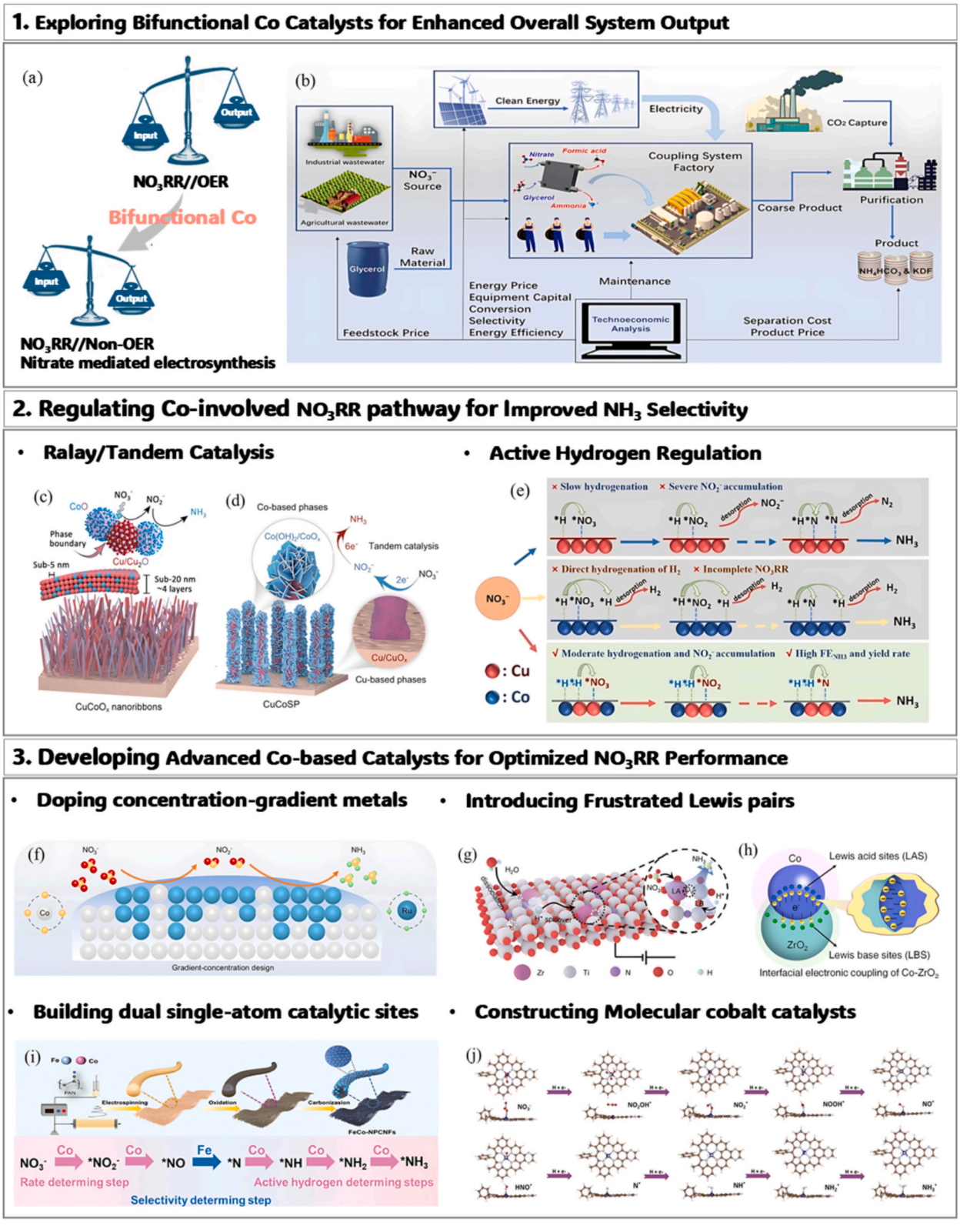

Fig. 11. Future prospects of Co-based catalysts for NO_3RR. (a) The coupled nitrate reduction with alternative anode reactions to enhance system output. (b) The coupled NO_3RR system together with up and downstream processes [159]. (c) Schematic illustration of the preparation of a CuCoOx based binary 'tandem catalyst' [162]. (d) Schematic illustration of the preparation of a Cu/Co-based binary 'tandem catalyst' [83]. (e) Proposed NO_3RR pathways of meso-Cu, meso-Co, and meso-CoCu. Reproduced with permission [164]. Copyright 2024, John Wiley and Sons. (f) Catalyst design of gradient-concentration RuCo electrocatalyst [166]. (g) Schematic illustration of the electrosynthesis of NH_3 by constructing FLPs on the surface of Zr-TiON catalysts. Reproduced with permission [169]. Copyright 2024, John Wiley and Sons. (h) Illustration of the active Lewis acid-base site pairs at the Co-ZrO_2 ND heterojunctions. Reproduced with permission [170]. Copyright 2024, American Chemical Society. (i) Schematic of the electrocatalytic NO_3RR to NH_3 under ambient conditions with renewable energy and schematic of FeCo-NPCNFs synthesis. Reproduced with permission [171]. Copyright 2024, John Wiley and Sons. (j) Illustration of reaction path on CoQPyPhenI [173].

nanosheets (RuCo) for efficient nitrate reduction at low concentrations (Fig. 11f) [166]. This electrocatalyst achieved an optimal NH_3 FE of more than 93 % at an industrial-scale current density of 1.0 A cm^{-2} in a 2000 ppm NO_3^- electrolyte, with stable performance over 720 h at −300 mA cm^{-2}. The RuCo catalyst also maintained robust reactivity in a 62 ppm NO_3^- electrolyte.

Since NO_3^- is a Lewis base (LB), generating Lewis acid (LA) sites with electron-deficient features would help NO_3^- interact favorably with the catalyst and promote NO_3^- dissociation and activation. Moreover, since two H^+ also function as Lewis acids, positively charged LA sites can prevent the HER by interfering with the reduction of two H^+ to H_2 through electrostatic repulsion [167]. Frustrated Lewis pairs (FLPs) consist of electron-deficient LA and electron-accepting LB that are spatially prevented from forming bonds, allowing them to chemisorb and react with various ions [168]. Yang et al. prepared N-doped TiO_{2-x} supported by Zr single atoms (Zr-TiON) with rich oxygen vacancies (O_v), in which unsaturated Zr (LA) sites together with oxygen atoms around O_v (LB) formed frustrated FLPs [169]. Attributed to the strong LA of the Zr single atom, NO_3^- spontaneously adsorbed at the Zr site, while H_2O molecules were cleaved to *H by the enhanced FLPs and adsorbed at the LB of the O atom around O_v. Eventually electrical energy acted as the driving force for the proton-coupled electron transfer process to produce NH_3 and released it from the catalyst surface (Fig. 11g). Co-based catalysts featuring FLPs exhibit exceptional catalytic activity in various reactions by leveraging synergistic interactions between Lewis acid and base sites, which enhance reactant activation and conversion efficiency. For example, Cui et al. demonstrated that an FLPs system was composed of independent Co metal center and N sites in defective Co_3O_4@NC, which can effectively activate cinnamaldehyde and isopropanol and reduce the activation energy barrier. Ma et al. reported a stable Co-ZrO_2 metal-semiconductor heterojunction electrocatalyst, fabricated by assembling electron-coupled Co-ZrO_2 nanodots into macroporous carbon nanofibers (Fig. 11h) [170]. The Co-ZrO_2 interface enriched electrons, facilitating electron transfer from Co to ZrO_2, which generated LA sites on Co for polysulfide adsorption. Simultaneously, interfacial electrons activated the S—S bond, accelerating long-chain polysulfide conversion, while ZrO_2's LB sites promoted short-chain polysulfide desorption. Given these findings, the unique electronic and structural properties of Co-based electrocatalysts with FLPs suggest their great potential for NO_3RR.

Compared with SACs, dual-atom catalysts (DACs) have higher metal loading and more complex and flexible active sites, thus achieving better catalytic performance and providing more opportunities for electrocatalysis. For example, Luo et al. synthesized FeCo alloy confined within nitrogen-doped porous carbon nanofibers (FeCo-NPCNFs), enabling relay catalysis between Fe and Co in NO_3RR (Fig. 11i) [171]. DFT calculations revealed that the incorporation of Co active sites not only modulates the d-band center of the FeCo alloy and optimizes intermediate adsorption but also enhances the supply of active hydrogen species, further improving catalytic efficiency.

Molecular catalysts have gained significant attention as promising candidates for promoting nitrate conversion to NH_3. Their key advantage lies in their well-defined structures, which allow precise control over reaction pathways through the strategic design of active centers [172]. For instance, Sun et al. employed cobalt-based molecular catalysts modified by different coordinating subunits, revealing that different coordination environments altered electronic structures and impacted NO_3RR activity [173]. Among the studied complexes, cobalt 7,10-Di(quinolin-8-yl)Pyrazino[2,3-f][1,10]Phenanthroline (CoQPyPhenI) with an N_2(pyridine)-N_2(pyrrole) core exhibited superior NH_3 selectivity and activity. Magnetic moment measurements established a correlation between turnover frequency and effective magnetic moments, linking activity to electronic structure. Computational analysis further showed that the rate-determining step energy aligns with calculated magnetic moments and d-band center, reinforcing the electronic structure's role in reactivity (Fig. 11j).

4.4. Practical application of NO_3RR towards sustainable ammonia production

In practical industrial applications such as wastewater treatment, nitrate often exists at relatively low concentrations (typically <50 mg NO_3-N L^{-1}). However, current lab-scale electrocatalytic systems are generally optimized under high nitrate concentrations, which limits their direct applicability in real-world scenarios. Additionally, various co-constituents, including organic and inorganic ions, suspended solids, and organic carbon, could compete for catalyst active sites, degrade materials, and disrupt optimal reaction conditions. Future research should therefore focus on developing highly active, selective, and stable catalysts capable of efficiently operating in realistic low-concentration nitrate wastewater. To address the electrostatic repulsion between NO_3^- ions and the cathode surface under dilute conditions, Xue et al. designed hydrophilic Cu@$CuCoO_2$ nano-islands dispersed on a conductive support [174]. This architecture significantly enhanced NO_3^- adsorption and promoted ammonia synthesis via dynamic Cu—Co redox site evolution. When tested in natural NO_3^--contaminated water streams (48.9 mg-N L^{-1}), the catalyst exhibited excellent performance, achieving an NH_3 selectivity of 93.5 %, NO_3^- conversion of 96.1 %, and low energy consumption of 0.079 kWh gNH_3^{-1}, demonstrating its strong potential for treating diluted nitrate streams efficiently.

Another critical challenge for the industrial application of NO_3RR lies in the efficient separation and recovery of the produced ammonia from the electrolyte, which remains particularly non-trivial in diluted aqueous systems due to the low concentration and high solubility of ammonia. Strategies such as membrane-based separation, in-situ stripping, and gas-extraction electrode could be integrated to improve the overall process efficiency. For example, a hybrid flow reactor was developed that allowed for the simultaneous removal of nitrate pollutants and recovery of ammonia [175]. The reactor consisted of three main compartments: a trap chamber, a wastewater chamber, and an anode chamber, separated by a self-standing Co@Cu electrode supported on a polytetrafluoroethylene (PTFE) membrane. During the electrocatalytic nitrate reduction reaction, the local consumption of protons near the Co@Cu electrode induced a high local pH, creating an alkaline microenvironment adjacent to the PTFE membrane. When an acidic solution was introduced into the trap chamber, the resulting pH gradient across the membrane drived the diffusion of ammonia gas from the wastewater side into the trap chamber. Additionally, a PEM-free flow-through electrochemical cell was employed, incorporating a 3D-printed MPCN cathode and a homemade IrO_2-Ta_2O_5 coated Ti anode, which exhibited excellent stability in complex wastewater environments [176]. A gas stripping technique was adopted for the in-situ collection of ammonia, with UV irradiation (254 nm) integrated into the stripping unit to simultaneously suppress ammonia oxidation caused by hypochlorite (ClO^-) in chloride-rich wastewater. UV light effectively decomposed ClO^- into reactive radicals (Cl• and •OH), which preferentially reacted with other impurities, thereby limiting NH_4^+ oxidation to improve ammonia recovery efficiency. Gao et al. also developed a membrane-free electrolyzer equipped with gas-extraction electrodes that enabled the simultaneous production and separation of NH_3 and Cl_2 [177]. The key innovation lied in the electrode architecture, which integrated an electrocatalyst layer with a gas exchange layer, allowing for efficient in-situ capture of gaseous products. Furthermore, a stacked electrolyzer system comprising three modules with a total electrode area of 300 cm^2 was successfully implemented to treat actual reverse osmosis retentate. This system produced concentrated end-products—$(NH_4)_2SO_4$ (83.8 mM) and NaClO (243.4 mM)—while maintaining low residual concentrations of reactive intermediates and target compounds (NH_3/NH_4^+: 0.3 mM, NO_2^-: 0.2 mM, Cl_2/HClO/ClO^-: 0.1 mM), demonstrating its effectiveness for ammonia recovery and wastewater treatment.

Furthermore, techno-economic analysis (TEA) and life-cycle analysis (LCA) are needed to evaluate the commercial viability and

environmental impact of electrocatalytic nitrate-to-ammonia conversion systems. For instance, Zhang et al. conducted a preliminary TEA and LCA using NO_3^- rich wastewater from an electroplating facility as a representative case [176]. Traditional treatment methods, which involved evaporation, crystallization, solidification, and landfill, incurred high operational costs—exceeding US$193.50 per m^3—primarily due to solidification, equipment maintenance, and energy-intensive evaporation processes. In contrast, the electrochemical NO_3^- conversion synchronized with NH_3 recovery (ECSN) system significantly reduced the treatment cost to US$116.30 per m^3, mainly attributed to electrochemical ammonia conversion and recovery. This cost can be further lowered to US$105.00 per m^3 when accounting for the value of recovered NH_3-N, highlighting its economic competitiveness. From an environmental standpoint, the ECSN system demonstrated marked superiority over conventional treatment methods in terms of emissions reduction, resource efficiency, and ecological impact mitigation. Compared with traditional methods, it reduced global warming potential by over 60 %, terrestrial ecotoxicity by 84 %, and human non-carcinogenic toxicity by 49 %, largely due to the elimination of high-temperature and cement-based processes. When powered by clean energy sources such as wind, solar, or nuclear, the system's carbon emissions can be further decreased by up to 25-fold. Additionally, the risk of NO_3^- leakage into water bodies was eliminated, significantly lowering marine eutrophication potential. On a global scale, the implementation of ECSN may have the potential to recover approximately 1.26 million tons of NH_3 annually from nitrate-rich wastewaters, which could avoid up to 207 million tons of CO_2 emissions associated with conventional wastewater treatment and ammonia production via the Habe-Bosch process.

5. Conclusions

This review highlights the potential of cobalt-based electrocatalysts as a promising strategy for electrochemical nitrate reduction to ammonia, offering a sustainable alternative to the energy-intensive Haber-Bosch process. Significant advancements in catalyst design—including doping strategies, defect engineering, heterostructure construction, and in-situ reconstruction—have greatly improved catalytic activity and selectivity. Moreover, mechanistic insights into NO_3RR pathways, the role of Co active sites, and electronic structure modulation have provided a deeper understanding of the structure–performance relationship of Co-based electrocatalysts. These findings offer valuable guidance for the rational design and optimization of Co-based catalysts for enhanced NO_3RR performance. Despite these advancements, challenges remain in improving ammonia selectivity, suppressing competing reactions, and maintaining long-term catalyst stability under realistic operating conditions. Future research should focus on developing bifunctional catalysts that enable alternative anodic reactions for improved system efficiency, optimizing catalytic pathways to enhance ammonia selectivity, and leveraging emerging strategies for more insight into Co reactivity. By tackling these issues, Co-based NO_3RR catalysts can pave the way for more efficient and sustainable ammonia production, ultimately contributing to a greener nitrogen cycle.

Declaration of competing interest

The authors declare that they have no known competing financial interests or personal relationships that could have appeared to influence the work reported in this paper.

Acknowledgements

This work was supported by the Australian Research Council (ARC) Projects (DP220101139, DP220101142, and LP240100542).

Appendix A. Supplementary data

Supplementary data to this article can be found online at https://doi.org/10.1016/j.ccr.2025.216751.

Data availability

No data was used for the research described in the article.

References

[1] D.E. Canfield, A.N. Glazer, P.G. Falkowski, The evolution and future of earth's nitrogen cycle, Science 330 (2010) 192–196, https://doi.org/10.1126/science.1186120.
[2] J.A. Camargo, Á. Alonso, Ecological and toxicological effects of inorganic nitrogen pollution in aquatic ecosystems: a global assessment, Environ. Int. 32 (2006) 831–849, https://doi.org/10.1016/j.envint.2006.05.002.
[3] S. Dey, G.T. Naga Veerendra, A.V. Phani Manoj, S.S. Anjaneya Babu Padavala, Invasive lignocellulose-based plants bio-sorbents for the elimination of nitrites of emerging concern from water, Environ. Funct. Mater. 2 (2023) 255–274, https://doi.org/10.1016/j.efmat.2024.05.002.
[4] L. Knobeloch, B. Salna, A. Hogan, J. Postle, H. Anderson, Blue babies and nitrate-contaminated well water, Environ. Health Perspect. 108 (2000) 675–678, https://doi.org/10.1289/ehp.00108675.
[5] B. Van Der Bruggen, C. Vandecasteele, T. Van Gestel, W. Doyen, R. Leysen, A review of pressure-driven membrane processes in wastewater treatment and drinking water production, Environ. Prog. 22 (2003) 46–56, https://doi.org/10.1002/ep.670220116.
[6] M.B. Jackson, B.A. Bolto, Effect of ion-exchange resin structure on nitrate selectivity, React. Polym. 12 (1990) 277–290, https://doi.org/10.1016/0923-1137(90)90078-I.
[7] A. Bhatnagar, M. Sillanpää, A review of emerging adsorbents for nitrate removal from water, Chem. Eng. J. 168 (2011) 493–504, https://doi.org/10.1016/j.cej.2011.01.103.
[8] H. Nassrullah, S.F. Anis, R. Hashaikeh, N. Hilal, Energy for desalination: a state-of-the-art review, Desalination 491 (2020) 114569, https://doi.org/10.1016/j.desal.2020.114569.
[9] B. Van der Bruggen, C. Vandecasteele, Removal of pollutants from surface water and groundwater by nanofiltration: overview of possible applications in the drinking water industry, Environ. Pollut. 122 (2003) 435–445, https://doi.org/10.1016/S0269-7491(02)00308-1.
[10] M. Palencia, B.L. Rivas, Adsorption of linear polymers on polyethersulfone membranes: contribution of divalent counterions on modifying of hydrophilic–lipophilic balance of polyelectrolyte chain, J. Membr. Sci. 372 (2011) 355–365, https://doi.org/10.1016/j.memsci.2011.02.023.
[11] S.S. Madaeni, The application of membrane technology for water disinfection, Water Res. 33 (1999) 301–308, https://doi.org/10.1016/S0043-1354(98)00212-7.
[12] C. Gabaldón, M. Izquierdo, V. Martínez-Soria, P. Marzal, J.-M. Penya-roja, F. Javier Alvarez-Hornos, Biological nitrate removal from wastewater of a metal-finishing industry, J. Hazard. Mater. 148 (2007) 485–490, https://doi.org/10.1016/j.jhazmat.2007.02.071.
[13] X. Lv, H. Peng, X. Wang, L. Hu, M. Peng, Z. Liu, G. Jiang, Nitrate reduction by nanoscale zero valent iron (nFe0)-based systems: mechanism, reaction pathway and strategy for enhanced N2 formation, Chem. Eng. J. 430 (2022) 133133, https://doi.org/10.1016/j.cej.2021.133133.
[14] Y. Cao, S. Yuan, L. Meng, Y. Wang, Y. Hai, S. Su, W. Ding, Z. Liu, X. Li, M. Luo, Recent advances in Electrocatalytic nitrate reduction to Ammonia: mechanism insight and catalyst design, ACS Sustain. Chem. Eng. 11 (2023) 7965–7985, https://doi.org/10.1021/acssuschemeng.3c01084.
[15] W. Yang, J. Wang, R. Chen, L. Xiao, S. Shen, J. Li, F. Dong, Reaction mechanism and selectivity regulation of photocatalytic nitrate reduction for wastewater purification: progress and challenges, J. Mater. Chem. A 10 (2022) 17357–17376, https://doi.org/10.1039/D2TA04611C.
[16] Q. Wu, F. Zhu, G. Wallace, X. Yao, J. Chen, Electrocatalysis of nitrogen pollution: transforming nitrogen waste into high-value chemicals, Chem. Soc. Rev. 53 (2024) 557–565, https://doi.org/10.1039/D3CS00714F.
[17] B.H.R. Suryanto, H.-L. Du, D. Wang, J. Chen, A.N. Simonov, D.R. MacFarlane, Challenges and prospects in the catalysis of electroreduction of nitrogen to ammonia, Nat. Catal. 2 (2019) 290–296, https://doi.org/10.1038/s41929-019-0252-4.
[18] R.F. Service, New recipe produces ammonia from air, water, and sunlight, Science 345 (2014) 610, https://doi.org/10.1126/science.345.6197.610.
[19] D.R. MacFarlane, P.V. Cherepanov, J. Choi, B.H.R. Suryanto, R.Y. Hodgetts, J. M. Bakker, F.M. Ferrero Vallana, A.N. Simonov, A roadmap to the Ammonia economy, Joule 4 (2020) 1186–1205, https://doi.org/10.1016/j.joule.2020.04.004.
[20] J.G. Chen, R.M. Crooks, L.C. Seefeldt, K.L. Bren, R.M. Bullock, M.Y. Darensbourg, P.L. Holland, B. Hoffman, M.J. Janik, A.K. Jones, M.G. Kanatzidis, P. King, K. M. Lancaster, S.V. Lymar, P. Pfromm, W.F. Schneider, R.R. Schrock, Beyond fossil fuel–driven nitrogen transformations, Science 360 (2018) eaar6611, https://doi.org/10.1126/science.aar6611.

[21] K.H.R. Rouwenhorst, A.G.J. Van Der Ham, G. Mul, S.R.A. Kersten, Islanded ammonia power systems: technology review & conceptual process design, Renew. Sust. Energ. Rev. 114 (2019) 109339, https://doi.org/10.1016/j.rser.2019.109339.
[22] M.A. Shipman, M.D. Symes, Recent progress towards the electrosynthesis of ammonia from sustainable resources, Catal. Today 286 (2017) 57–68, https://doi.org/10.1016/j.cattod.2016.05.008.
[23] X. Cao, J. Huo, L. Li, J. Qu, Y. Zhao, W. Chen, C. Liu, H. Liu, G. Wang, Recent advances in engineered Ru-based Electrocatalysts for the hydrogen/oxygen conversion reactions, Adv. Energy Mater. 12 (2022) 2202119, https://doi.org/10.1002/aenm.202202119.
[24] Y. Xiong, Y. Wang, J. Zhou, F. Liu, F. Hao, Z. Fan, Electrochemical nitrate reduction: ammonia synthesis and the beyond, Adv. Mater. 36 (2024) 2304021, https://doi.org/10.1002/adma.202304021.
[25] B.H. Ko, B. Hasa, H. Shin, Y. Zhao, F. Jiao, Electrochemical reduction of gaseous nitrogen oxides on transition metals at ambient conditions, J. Am. Chem. Soc. 144 (2022) 1258–1266, https://doi.org/10.1021/jacs.1c10535.
[26] Z. Wu, Y. Song, Y. Liu, W. Luo, W. Li, J. Yang, Electrocatalytic nitrate reduction: selectivity at the crossroads between ammonia and nitrogen, Chem Catal. 3 (2023), https://doi.org/10.1016/j.checat.2023.100786.
[27] S. Niu, J. Yang, L. Qian, D. Zhou, P. Du, N. Si, X. Gu, D. Jiang, Y. Feng, Electrochemical nitrate reduction to Ammonia - recent Progress, ChemElectroChem 10 (2023) e202300419, https://doi.org/10.1002/celc.202300419.
[28] C. Smith, A.K. Hill, L. Torrente-Murciano, Current and future role of Haber-Bosch ammonia in a carbon-free energy landscape, Energy Environ. Sci. 13 (2020) 331–344, https://doi.org/10.1039/C9EE02873K.
[29] H. Xu, Y. Ma, J. Chen, W. Zhang, J. Yang, Electrocatalytic reduction of nitrate – a step towards a sustainable nitrogen cycle, Chem. Soc. Rev. 51 (2022) 2710–2758, https://doi.org/10.1039/D1CS00857A.
[30] Y. Yu, Y. Li, Y. Fang, L. Wen, B. Tu, Y. Huang, Recent advances of ammonia synthesis under ambient conditions over metal-organic framework based electrocatalysts, Appl. Catal. B Environ. 340 (2024) 123161, https://doi.org/10.1016/j.apcatb.2023.123161.
[31] W. Wen, S. Fang, Y. Zhou, Y. Zhao, P. Li, X.-Y. Yu, Modulating the electrolyte microenvironment in electrical double layer for boosting Electrocatalytic nitrate reduction to Ammonia, Angew. Chem. 136 (2024) e202408382, https://doi.org/10.1002/ange.202408382.
[32] J.M. McEnaney, S.J. Blair, A.C. Nielander, J.A. Schwalbe, D.M. Koshy, M. Cargnello, T.F. Jaramillo, Electrolyte engineering for efficient electrochemical nitrate reduction to Ammonia on a titanium electrode, ACS Sustain. Chem. Eng. 8 (2020) 2672–2681, https://doi.org/10.1021/acssuschemeng.9b05983.
[33] L. Barrera, R. Silcox, K. Giammalvo, E. Brower, E. Isip, R. Bala Chandran, Combined effects of concentration, pH, and polycrystalline copper surfaces on Electrocatalytic nitrate-to-Ammonia activity and selectivity, ACS Catal. 13 (2023) 4178–4192, https://doi.org/10.1021/acscatal.2c05136.
[34] J. Guo, P. Brimley, M.J. Liu, E.R. Corson, C. Muñoz, W.A. Smith, W.A. Tarpeh, Mass transport modifies the interfacial electrolyte to influence electrochemical nitrate reduction, ACS Sustain. Chem. Eng. 11 (2023) 7882–7893, https://doi.org/10.1021/acssuschemeng.3c01057.
[35] Y.-T. Xu, Z. Peng, Y. Han, H. Zhong, J. Yang, Y. Cao, Insight into hydrogenation selectivity of the Electrocatalytic nitrate-to-Ammonia reduction reaction via enhancing the proton transport, ChemSusChem 15 (2022) e202102450, https://doi.org/10.1002/cssc.202102450.
[36] Z.-Y. Yang, Y.-D. Li, D. Liu, M.-S. Song, Y. Gao, Q.-P. Wu, E.-S. Han, Y.-Z. He, X.-H. Yang, Engineering CuMn Prussian blue analog-shelled nanobox for efficient electrochemical reduction of nitrate to ammonia, Tungsten 6 (2024) 833–844, https://doi.org/10.1007/s42864-024-00275-z.
[37] X. Zhang, Y. Wang, C. Liu, Y. Yu, S. Lu, B. Zhang, Recent advances in non-noble metal electrocatalysts for nitrate reduction, Chem. Eng. J. 403 (2021) 126269, https://doi.org/10.1016/j.cej.2020.126269.
[38] S. Li, X. Wang, X. Chi, Y. Xiong, Y. Sun, Z. Tang, X. Gao, H. Zhang, J. Li, K. Nie, J. Xie, Z. Yang, Y.-M. Yan, Boosted N2 activation through 4f–2p–3d orbital hybridization for efficient nitrate Electrosynthesis, Adv. Funct. Mater. 33 (2023) 2306098, https://doi.org/10.1002/adfm.202306098.
[39] X. Liang, H. Zhu, X. Yang, S. Xue, Z. Liang, X. Ren, A. Liu, G. Wu, Recent advances in designing efficient Electrocatalysts for electrochemical nitrate reduction to Ammonia, Small Struct. 4 (2023) 2200202, https://doi.org/10.1002/sstr.202200202.
[40] H. Zhang, H. Wang, X. Cao, M. Chen, Y. Liu, Y. Zhou, M. Huang, L. Xia, Y. Wang, T. Li, D. Zheng, Y. Luo, S. Sun, X. Zhao, X. Sun, Unveiling cutting-edge developments in Electrocatalytic nitrate-to-Ammonia conversion, Adv. Mater. 36 (2024) 2312746, https://doi.org/10.1002/adma.202312746.
[41] C. Wang, Y. Zhang, H. Luo, H. Zhang, W. Li, W. Zhang, J. Yang, Iron-based Nanocatalysts for electrochemical nitrate reduction, Small Methods 6 (2022) 2200790, https://doi.org/10.1002/smtd.202200790.
[42] Z.-Y. Wu, M. Karamad, X. Yong, Q. Huang, D.A. Cullen, P. Zhu, C. Xia, Q. Xiao, M. Shakouri, F.-Y. Chen, J.Y. Timothy Kim, Y. Xia, K. Heck, Y. Hu, M.S. Wong, Q. Li, I. Gates, S. Siahrostami, H. Wang, Electrochemical ammonia synthesis via nitrate reduction on Fe single atom catalyst, Nat. Commun. 12 (2021) 2870, https://doi.org/10.1038/s41467-021-23115-x.
[43] S. Ullah, S. Wang, C. Li, A. Ullah Jan, F. Zhan, H.M.A. Sharif, Q. Liu, G. Wang, Recent developments in designing cu-based electrocatalysts and advanced strategies for electrochemical nitrate reduction to ammonia, J. Environ. Chem. Eng. 11 (2023) 110927, https://doi.org/10.1016/j.jece.2023.110927.
[44] T. Ren, Y. Sheng, M. Wang, K. Ren, L. Wang, Y. Xu, Recent advances of cu-based materials for electrochemical nitrate reduction to Ammonia, Chin. J. Struct. Chem. 41 (2022) 2212089–2212106, https://doi.org/10.14102/j.cnki.0254-5861.2022-0201.
[45] I.M. Ul Hasan, N. Xu, Y. Liu, M.Z. Nawaz, H. Feng, J. Qiao, Noble and non-Noble metal based catalysts for electrochemical nitrate reduction to Ammonia: activity, selectivity and stability, Electrochem. Energy Rev. 7 (2024) 36, https://doi.org/10.1007/s41918-024-00236-7.
[46] Z.-L. Xie, D. Wang, X.-Q. Gong, Theoretical insights into nitrate reduction to Ammonia over Pt/TiO2: reaction mechanism, activity regulation, and catalyst design, ACS Catal. 12 (2022) 9887–9896, https://doi.org/10.1021/acscatal.2c01694.
[47] Z. Chen, N. Han, R. Zheng, Z. Ren, W. Wei, B. Ni, Design of earth-abundant amorphous transition metal-based catalysts for electrooxidation of small molecules: advances and perspectives, SusMat 3 (2023) 290–319, https://doi.org/10.1002/sus2.131.
[48] J. Zhao, B. Shang, J. Zhai, N-doped graphene as an efficient metal-free Electrocatalyst for indirect nitrate reduction reaction, Nanomaterials 11 (2021) 2418, https://doi.org/10.3390/nano11092418.
[49] H. Yin, X. Mao, S. Bell, D. Golberg, A. Du, Transition-metal-free, pure p-block alloy Electrocatalysts for the highly efficient nitrate reduction to Ammonia, Chem. Mater. 35 (2023) 2884–2891, https://doi.org/10.1021/acs.chemmater.2c03788.
[50] Q. Wu, W. Zhu, D. Ma, C. Liang, Z. Wang, H. Liang, Screening of transition metal oxides for electrocatalytic nitrate reduction to ammonia at large currents, Nano Res. 17 (2024) 3902–3910, https://doi.org/10.1007/s12274-023-6379-2.
[51] Y. Wu, K.-K. Lu, L.-H. Xu, Progress and prospects of electrochemical reduction of nitrate to restore the nitrogen cycle, J. Mater. Chem. A 11 (2023) 17392–17417, https://doi.org/10.1039/D3TA01592K.
[52] W. Chen, X. Yang, Z. Chen, Z. Ou, J. Hu, Y. Xu, Y. Li, X. Ren, S. Ye, J. Qiu, J. Liu, Q. Zhang, Emerging applications, developments, prospects, and challenges of electrochemical nitrate-to-Ammonia conversion, Adv. Funct. Mater. 33 (2023) 2300512, https://doi.org/10.1002/adfm.202300512.
[53] Q. Yan, R. Zhao, L. Yu, Z. Zhao, L. Liu, J. Xi, Enhancing compatibility of two-step tandem catalytic nitrate reduction to Ammonia over P-cu/co(OH)2, Adv. Mater. 36 (2024) 2408680, https://doi.org/10.1002/adma.202408680.
[54] S. Zheng, X. Yang, Z.-Z. Shi, H. Ding, F. Pan, J.-F. Li, The loss of interfacial water-adsorbate hydrogen bond connectivity position surface-active hydrogen as a crucial intermediate to enhance nitrate reduction reaction, J. Am. Chem. Soc. 146 (2024) 26965–26974, https://doi.org/10.1021/jacs.4c08256.
[55] Y. Li, Z. Lu, L. Zheng, X. Yan, J. Xie, Z. Yu, S. Zhang, F. Jiang, H. Chen, The synergistic catalysis effect on electrochemical nitrate reduction at the dual-function active sites of the heterostructure, Energy Environ. Sci. 17 (2024) 4582–4593, https://doi.org/10.1039/D4EE00784K.
[56] K. Fan, W. Xie, J. Li, Y. Sun, P. Xu, Y. Tang, Z. Li, M. Shao, Active hydrogen boosts electrochemical nitrate reduction to ammonia, Nat. Commun. 13 (2022) 7958, https://doi.org/10.1038/s41467-022-35664-w.
[57] X. Deng, Y. Yang, L. Wang, X.-Z. Fu, J.-L. Luo, Metallic co Nanoarray catalyzes selective NH3 production from electrochemical nitrate reduction at current densities exceeding 2 a cm-2, Adv. Sci. 8 (2021) 2004523, https://doi.org/10.1002/advs.202004523.
[58] J. Yan, H. Xu, L. Chang, A. Lin, D. Cheng, Revealing the pH-dependent mechanism of nitrate electrochemical reduction to ammonia on single-atom catalysts, Nanoscale 14 (2022) 15422–15431, https://doi.org/10.1039/D2NR02545K.
[59] J. Chen, T. Gong, Q. Hou, J. Li, L. Zhang, D. Zhao, Y. Luo, D. Zheng, T. Li, S. Sun, Z. Cai, Q. Liu, L. Xie, M. Wu, A.A. Alshehri, X. Sun, Co/N-doped carbon nanospheres derived from an adenine-based metal organic framework enabled high-efficiency electrocatalytic nitrate reduction to ammonia, Chem. Commun. 58 (2022) 13459–13462, https://doi.org/10.1039/D2CC05333K.
[60] H. Liu, J. Qin, J. Mu, B. Liu, In situ interface engineered co/NC derived from ZIF-67 as an efficient electrocatalyst for nitrate reduction to ammonia, J. Colloid Interface Sci. 636 (2023) 134–140, https://doi.org/10.1016/j.jcis.2023.01.014.
[61] S. Ye, Z. Chen, G. Zhang, W. Chen, C. Peng, X. Yang, L. Zheng, Y. Li, X. Ren, H. Cao, D. Xue, J. Qiu, Q. Zhang, J. Liu, Elucidating the activity, mechanism and application of selective electrosynthesis of ammonia from nitrate on cobalt phosphide, Energy Environ. Sci. 15 (2022) 760–770, https://doi.org/10.1039/D1EE03097C.
[62] H. Zhang, G. Wang, C. Wang, Y. Liu, Y. Yang, C. Wang, W. Jiang, L. Fu, J. Xu, CoP nanowires on carbon cloth for electrocatalytic NOx- reduction to ammonia, J. Electroanal. Chem. 910 (2022) 116171, https://doi.org/10.1016/j.jelechem.2022.116171.
[63] J. Lu, S. Lv, H.S. Park, Q. Chen, Electrocatalytically active and charged natural chalcopyrite for nitrate-contaminated wastewater purification extended to energy storage Zn-NO3- battery, J. Hazard. Mater. 477 (2024) 135287, https://doi.org/10.1016/j.jhazmat.2024.135287.
[64] C. Xu, B. Li, H. Du, F. Kang, Energetic zinc ion chemistry: the rechargeable zinc ion battery, Angew. Chem. Int. Ed. 51 (2012) 933–935, https://doi.org/10.1002/anie.201106307.
[65] R. Zhang, H. Hong, X. Liu, S. Zhang, C. Li, H. Cui, Y. Wang, J. Liu, Y. Hou, P. Li, Z. Huang, Y. Guo, C. Zhi, Molecular engineering of a metal-organic polymer for enhanced electrochemical nitrate-to-Ammonia conversion and zinc nitrate batteries, Angew. Chem. Int. Ed. 62 (2023) e202309930, https://doi.org/10.1002/anie.202309930.
[66] Z. Deng, J. Liang, Q. Liu, C. Ma, L. Xie, L. Yue, Y. Ren, T. Li, Y. Luo, N. Li, B. Tang, A. Ali Alshehri, I. Shakir, P.O. Agboola, S. Yan, B. Zheng, J. Du, Q. Kong, X. Sun,

High-efficiency ammonia electrosynthesis on self-supported Co2AlO4 nanoarray in neutral media by selective reduction of nitrate, Chem. Eng. J. 435 (2022) 135104, https://doi.org/10.1016/j.cej.2022.135104.
[67] Q. Liu, L. Xie, J. Liang, Y. Ren, Y. Wang, L. Zhang, L. Yue, T. Li, Y. Luo, N. Li, B. Tang, Y. Liu, S. Gao, A.A. Alshehri, I. Shakir, P.O. Agboola, Q. Kong, Q. Wang, D. Ma, X. Sun, Ambient Ammonia synthesis via electrochemical reduction of nitrate enabled by NiCo2O4 nanowire Array, Small 18 (2022) 2106961, https://doi.org/10.1002/smll.202106961.
[68] X. Xu, L. Hu, Z. Li, L. Xie, S. Sun, L. Zhang, J. Li, Y. Luo, X. Yan, M.S. Hamdy, Q. Kong, X. Sun, Q. Liu, Oxygen vacancies in Co3O4 nanoarrays promote nitrate electroreduction for ammonia synthesis, Sustain. Energy Fuel 6 (2022) 4130–4136, https://doi.org/10.1039/d2se00830k.
[69] F. Zhao, G. Hai, X. Li, Z. Jiang, H. Wang, Enhanced electrocatalytic nitrate reduction to ammonia on cobalt oxide nanosheets via multiscale defect modulation, Chem. Eng. J. 461 (2023) 141960, https://doi.org/10.1016/j.cej.2023.141960.
[70] P. Wei, J. Liang, Q. Liu, L. Xie, X. Tong, Y. Ren, T. Li, Y. Luo, N. Li, B. Tang, A. M. Asiri, M.S. Hamdy, Q. Kong, Z. Wang, X. Sun, Iron-doped cobalt oxide nanoarray for efficient electrocatalytic nitrate-to-ammonia conversion, J. Colloid Interface Sci. 615 (2022) 636–642, https://doi.org/10.1016/j.jcis.2022.01.186.
[71] Z. Niu, S. Fan, X. Li, Z. Liu, J. Wang, J. Duan, M.O. Tadé, S. Liu, Facile tailoring of the electronic structure and the d-band Center of Copper-Doped Cobaltate for efficient nitrate electrochemical hydrogenation, ACS Appl. Mater. Interfaces 14 (2022) 35477–35484, https://doi.org/10.1021/acsami.2c04789.
[72] Z. Niu, S. Fan, X. Li, P. Wang, Z. Liu, J. Wang, C. Bai, D. Zhang, Bifunctional copper-cobalt spinel electrocatalysts for efficient tandem-like nitrate reduction to ammonia, Chem. Eng. J. 450 (2022) 138343, https://doi.org/10.1016/j.cej.2022.138343.
[73] D. Liu, L. Qiao, Y. Chen, P. Zhou, J. Feng, C.C. Leong, K.W. Ng, S. Peng, S. Wang, W.F. Ip, H. Pan, Electrocatalytic reduction of nitrate to ammonia on low-cost manganese-incorporated Co3O4 nanotubes, Appl. Catal. B Environ. 324 (2023) 122293, https://doi.org/10.1016/j.apcatb.2022.122293.
[74] J. Li, D. Zhao, L. Zhang, L. Yue, Y. Luo, Q. Liu, N. Li, A. Ali Alshehri, M.S. Hamdy, Q. Li, X. Sun, A FeCo 2 O 4 nanowire array enabled electrochemical nitrate conversion to ammonia, Chem. Commun. 58 (2022) 4480–4483, https://doi.org/10.1039/D2CC00189F.
[75] Z. Li, J. Liang, Q. Liu, L. Xie, L. Zhang, Y. Ren, L. Yue, N. Li, B. Tang, A. A. Alshehri, M.S. Hamdy, Y. Luo, Q. Kong, X. Sun, High-efficiency ammonia electrosynthesis via selective reduction of nitrate on ZnCo2O4 nanosheet array, Mater. Today Phys. 23 (2022) 100619, https://doi.org/10.1016/j.mtphys.2022.100619.
[76] Z. Niu, S. Fan, X. Li, J. Duan, A. Chen, Interfacial engineering of CoMn2O4/NC induced electronic delocalization boosts electrocatalytic nitrogen oxyanions reduction to ammonia, Appl. Catal. B Environ. 322 (2023) 122090, https://doi.org/10.1016/j.apcatb.2022.122090.
[77] Q.-L. Hong, J. Zhou, Q.-G. Zhai, Y.-C. Jiang, M.-C. Hu, X. Xiao, S.-N. Li, Y. Chen, Cobalt phosphide nanorings towards efficient electrocatalytic nitrate reduction to ammonia, Chem. Commun. 57 (2021) 11621–11624, https://doi.org/10.1039/D1CC04952F.
[78] Y. Jia, Y.-G. Ji, Q. Xue, F.-M. Li, G.-T. Zhao, P.-J. Jin, S.-N. Li, Y. Chen, Efficient nitrate-to-Ammonia Electroreduction at cobalt phosphide Nanoshuttles, ACS Appl. Mater. Interfaces 13 (2021) 45521–45527, https://doi.org/10.1021/acsami.1c12512.
[79] Q.-L. Hong, Z.-N. Zhang, X.-H. Wang, S.-B. Yin, F. Shi, S.-N. Li, Y. Chen, Iron-doped cobalt phosphide Nanohoops for Electroreduction of nitrate to Ammonia, Inorg. Chem. 61 (2022) 14397–14402, https://doi.org/10.1021/acs.inorgchem.2c02257.
[80] Z. Deng, C. Ma, X. Fan, Z. Li, Y. Luo, S. Sun, D. Zheng, Q. Liu, J. Du, Q. Lu, B. Zheng, X. Sun, Construction of CoP/TiO2 nanoarray for enhanced electrochemical nitrate reduction to ammonia, Mater. Today Phys. 28 (2022) 100854, https://doi.org/10.1016/j.mtphys.2022.100854.
[81] Z. Li, G. Wen, J. Liang, T. Li, Y. Luo, Q. Kong, X. Shi, A.M. Asiri, Q. Liu, X. Sun, High-efficiency nitrate electroreduction to ammonia on electrodeposited cobalt–phosphorus alloy film, Chem. Commun. 57 (2021) 9720–9723, https://doi.org/10.1039/D1CC02612G.
[82] S. Xu, Y. Shi, Z. Wen, X. Liu, Y. Zhu, G. Liu, H. Gao, L. Sun, F. Li, Polystyrene spheres-templated mesoporous carbonous frameworks implanted with cobalt nanoparticles for highly efficient electrochemical nitrate reduction to ammonia, Appl. Catal. B Environ. 323 (2023) 122192, https://doi.org/10.1016/j.apcatb.2022.122192.
[83] W. He, J. Zhang, S. Dieckhöfer, S. Varhade, A.C. Brix, A. Lielpetere, S. Seisel, J.R. C. Junqueira, W. Schuhmann, Splicing the active phases of copper/cobalt-based catalysts achieves high-rate tandem electroreduction of nitrate to ammonia, Nat. Commun. 13 (2022) 1129, https://doi.org/10.1038/s41467-022-28728-4.
[84] X. Fan, D. Zhao, Z. Deng, L. Zhang, J. Li, Z. Li, S. Sun, Y. Luo, D. Zheng, Y. Wang, B. Ying, J. Zhang, A.A. Alshehri, Y. Lin, C. Tang, X. Sun, Y. Zheng, Constructing Co@TiO2 Nanoarray Heterostructure with Schottky contact for selective Electrocatalytic nitrate reduction to Ammonia, Small 19 (2023) 2208036, https://doi.org/10.1002/smll.202208036.
[85] P. Huang, T. Fan, X. Ma, J. Zhang, Y. Zhang, Z. Chen, X. Yi, 3D flower-like zinc cobaltite for Electrocatalytic reduction of nitrate to Ammonia under ambient conditions, ChemSusChem 15 (2022) e202102049, https://doi.org/10.1002/cssc.202102049.
[86] T.H. Jeon, Z.-Y. Wu, F.-Y. Chen, W. Choi, P.J.J. Alvarez, H. Wang, et al., J. Phys. Chem. C 126 (2022) 6982–6989, https://doi.org/10.1021/acs.jpcc.1c10781.
[87] B. Yang, Y. Zhou, Z. Huang, B. Mei, Q. Kang, G. Chen, X. Liu, Z. Jiang, M. Liu, N. Zhang, Electron-deficient cobalt nanocrystals for promoted nitrate electrocatalytic reduction to synthesize ammonia, Nano Energy 117 (2023) 108901, https://doi.org/10.1016/j.nanoen.2023.108901.
[88] T. Xie, X. Li, J. Li, J. Chen, S. Sun, Y. Luo, Q. Liu, D. Zhao, C. Xu, L. Xie, X. Sun, Co nanoparticles decorated corncob-derived biomass carbon as an efficient Electrocatalyst for nitrate reduction to Ammonia, Inorg. Chem. 61 (2022) 14195–14200, https://doi.org/10.1021/acs.inorgchem.2c02499.
[89] J. Chen, Q. Zhou, L. Yue, D. Zhao, L. Zhang, Y. Luo, Q. Liu, N. Li, A.A. Alshehri, M. S. Hamdy, F. Gong, X. Sun, Co–NCNT nanohybrid as a highly active catalyst for the electroreduction of nitrate to ammonia, Chem. Commun. 58 (2022) 3787–3790, https://doi.org/10.1039/D2CC00245K.
[90] J. Wang, J. Liang, P. Liu, Z. Yan, L. Cui, L. Yue, L. Zhang, Y. Ren, T. Li, Y. Luo, Q. Liu, X.-E. Zhao, N. Li, B. Tang, Y. Liu, S. Gao, A.M. Asiri, H. Hao, R. Gao, X. Sun, Biomass Juncus derived carbon decorated with cobalt nanoparticles enables high-efficiency ammonia electrosynthesis by nitrite reduction, J. Mater. Chem. A 10 (2022) 2842–2848, https://doi.org/10.1039/D1TA09013E.
[91] R. Qi, Z. Wang, M. Zhong, C. Wang, F. Bai, X. Lu, Synergistic integration of amorphous cobalt phosphide with a Conductive Channel for highly efficient Electrocatalytic nitrate reduction to Ammonia, Small 20 (2024) 2308311, https://doi.org/10.1002/smll.202308311.
[92] L. Hu, D. Zhao, C. Liu, Y. Liang, D. Zheng, S. Sun, Q. Li, Q. Liu, Y. Luo, Y. Liao, L. Xie, X. Sun, Amorphous CoB nanoarray as a high-efficiency electrocatalyst for nitrite reduction to ammonia, Inorg. Chem. Front. 9 (2022) 6075–6079, https://doi.org/10.1039/D2QI01363K.
[93] J. Li, M. Li, N. An, S. Zhang, Q. Song, Y. Yang, J. Li, X. Liu, Boosted ammonium production by single cobalt atom catalysts with high faradic efficiencies, Proc. Natl. Acad. Sci. USA 119 (2022) e2123450119, https://doi.org/10.1073/pnas.2123450119.
[94] M. Song, Y. Xing, Y. Li, D. Liu, E. Han, Y. Gao, Z. Yang, X. Yang, Y. He, Fe and cu double-doped Co3O4 Nanorod with abundant oxygen vacancies: a high-rate Electrocatalyst for tandem Electroreduction of nitrate to Ammonia, Inorg. Chem. 62 (2023) 16641–16651, https://doi.org/10.1021/acs.inorgchem.3c02834.
[95] Q. Chen, J. Liang, Q. Liu, K. Dong, L. Yue, P. Wei, Y. Luo, Q. Liu, N. Li, B. Tang, A. A. Alshehri, M.S. Hamdy, Z. Jiang, X. Sun, Co nanoparticle-decorated pomelo-peel-derived carbon enabled high-efficiency electrocatalytic nitrate reduction to ammonia, Chem. Commun. 58 (2022) 4259–4262, https://doi.org/10.1039/D2CC00952H.
[96] D. Liu, L. Qiao, Y. Chen, P. Zhou, J. Feng, C.C. Leong, K.W. Ng, S. Peng, S. Wang, W.F. Ip, H. Pan, Electrocatalytic reduction of nitrate to ammonia on low-cost manganese-incorporated Co3O4 nanotubes, Appl. Catal. B Environ. 324 (2023) 122293, https://doi.org/10.1016/j.apcatb.2022.122293.
[97] N.C. Kani, N.H.L. Nguyen, K. Markel, R.R. Bhawnani, B. Shindel, K. Sharma, S. Kim, V.P. Dravid, V. Berry, J.A. Gauthier, M.R. Singh, Electrochemical reduction of nitrates on CoO nanoclusters-functionalized graphene with highest mass activity and nearly 100% selectivity to Ammonia, Adv. Energy Mater. 13 (2023) 2204236, https://doi.org/10.1002/aenm.202204236.
[98] C. Qin, B. Hou, J. Wang, G. Wang, Z. Ma, L. Jia, D. Li, Stabilizing optimal crystalline facet of cobalt catalysts for fischer–tropsch synthesis, ACS Appl. Mater. Interfaces 11 (2019) 33886–33893, https://doi.org/10.1021/acsami.9b10174.
[99] P. Jain, S. Gupta, C.P. Vinod, Role of exposed crystal facets in the atmospheric pressure CO hydrogenation on Co3O4 nanostructures, Nano-Struct. Nano-Objects 23 (2020) 100504, https://doi.org/10.1016/j.nanoso.2020.100504.
[100] S. Gupta, P. Jain, D. Jagadeesan, C.P. Vinod, Morphology-dependent catalysis by Co3O4 nanostructures in atmospheric pressure carbon dioxide hydrogenation, J. Phys. Chem. C 127 (2023) 13055–13064, https://doi.org/10.1021/acs.jpcc.3c02857.
[101] A. Zhu, H. Liu, S. Bu, K. Liu, C. Luan, D. Lin, G. Gan, Y. Zhou, T. Zhang, K. Liu, G. Hong, H. Li, W. Zhang, Facet-dependent evolution of active components on spinel Co3O4 for electrochemical Ammonia synthesis, ACS Nano 18 (2024) 22344–22355, https://doi.org/10.1021/acsnano.4c06637.
[102] S. Lu, G. Lin, H. Yan, Y. Li, T. Qi, Y. Li, S. Liang, L. Jiang, In situ facet transformation engineering over Co3O4 for highly efficient Electroreduction of nitrate to Ammonia, ACS Catal. 14 (2024) 14887–14894, https://doi.org/10.1021/acscatal.4c05292.
[103] W. Zhong, Y. Chen, P. Chen, Q. Chen, C. Yang, N. Zhang, X. Liu, Z. Lin, Balancing hydrogen evolution and hydrogenation reaction via facet engineering for efficient conversion of nitrate to Ammonia in actual wastewater, Angew. Chem. (2025) e202503117, https://doi.org/10.1002/ange.202503117.
[104] W. Lin, E. Zhou, J.-F. Xie, J. Lin, Y. Wang, A high power density Zn-nitrate electrochemical cell based on theoretically screened catalysts, Adv. Funct. Mater. 32 (2022) 2209464, https://doi.org/10.1002/adfm.202209464.
[105] P. Yang, M. Lü, D. Xü, D. Yuan, C. Song, G. Zhou, The effect of Co2+ and Co3+ on photoluminescence characteristics of ZnS nanocrystallines, J. Phys. Chem. Solids 62 (2001) 1181–1184, https://doi.org/10.1016/S0022-3697(00)00287-0.
[106] Z. Liu, X. Xia, H.-K. Guan, Q. Liu, S.-S. Zhao, X.-L. Cheng, Q.-Q. Xu, S.-S. Li, Hypersensitized electrochemical detection of hg(II) based on tunable sulfur-doped porous Co3O4 nanosheets: promotion Co2+/Co3+ valence change cycle and adsorption via introducing S, Chem. Eng. J. 435 (2022) 134950, https://doi.org/10.1016/j.cej.2022.134950.
[107] S.-S. Li, Q.-Q. Xu, J.-T. Xu, G. Yan, Y.-X. Zhang, S.-W. Li, L.-C. Yin, Engineering Co2+/Co3+ redox activity of Ni-mediated porous Co3O4 nanosheets for superior hg(II) electrochemical sensing: insight into the effect of valence change cycle and oxygen vacancy on electroanalysis, Sensors Actuators B Chem. 354 (2022) 131095, https://doi.org/10.1016/j.snb.2021.131095.

[108] X. Li, Y. Chen, X. Zhan, Y. Xu, L. Hao, L. Xu, X. Li, M. Umer, X. Tan, B. Han, A. W. Robertson, Z. Sun, Strategies for enhancing electrochemical CO2 reduction to multi-carbon fuels on copper, Innov. Mater. 1 (2023) 100014–100015, https://doi.org/10.59717/j.xinn-mater.2023.100014.
[109] Y. Tang, X. Li, H. Lv, D. Xie, W. Wang, C. Zhi, H. Li, Stabilized Co3+/Co4+ redox pair in in situ produced CoSe2−-derived cobalt oxides for alkaline Zn batteries with 10 000-cycle lifespan and 1.9-V voltage plateau, Adv. Energy Mater. 10 (2020) 2000892, https://doi.org/10.1002/aenm.202000892.
[110] J. Chen, W. Jia, X. Yu, Y. Sun, J. Zhang, S. Yang, X. Tang, L. Peng, X. Zeng, L. Lin, Insight into the Co2+/Co3+ sites for the selective reduction of furfural to furfuryl alcohol, Fuel 332 (2023) 126137, https://doi.org/10.1016/j.fuel.2022.126137.
[111] X.-L. Li, J. Bao, Z. Shadike, Q.-C. Wang, X.-Q. Yang, Y.-N. Zhou, D. Sun, F. Fang, Stabilizing transition metal vacancy induced oxygen redox by Co2+/Co3+ redox and sodium-site doping for layered cathode materials, Angew. Chem. Int. Ed. 60 (2021) 22026–22034, https://doi.org/10.1002/anie.202108933.
[112] J. Wang, R. Gao, D. Zhou, Z. Chen, Z. Wu, G. Schumacher, Z. Hu, X. Liu, Boosting the Electrocatalytic activity of Co3O4 Nanosheets for a Li-O2 battery through modulating inner oxygen vacancy and exterior Co3+/Co2+ ratio, ACS Catal. 7 (2017) 6533–6541, https://doi.org/10.1021/acscatal.7b02313.
[113] W. Fu, X. Du, P. Su, Q. Zhang, M. Zhou, Synergistic effect of co(III) and co(II) in a 3D structured Co3O4/carbon felt electrode for enhanced electrochemical nitrate reduction reaction, ACS Appl. Mater. Interfaces 13 (2021) 28348–28358, https://doi.org/10.1021/acsami.1c07063.
[114] O.Q. Carvalho, R. Marks, H.K.K. Nguyen, M.E. Vitale-Sullivan, S.C. Martinez, L. Árnadóttir, K.A. Stoerzinger, Role of electronic structure on nitrate reduction to ammonium: a periodic journey, J. Am. Chem. Soc. 144 (2022) 14809–14818, https://doi.org/10.1021/jacs.2c05673.
[115] Z. Song, Y. Chen, N. Ren, X. Duan, Recent advances in the fixed-electrode capacitive deionization (CDI): innovations in electrode materials and applications, Environ. Funct. Mater. 2 (2023) 290–303, https://doi.org/10.1016/j.efmat.2023.11.001.
[116] L. Xu, R. Iqbal, Y. Wang, S. Taimoor, L. Hao, R. Dong, K. Liu, J. Texter, Z. Sun, Emerging two-dimensional materials: synthesis, physical properties, and application for catalysis in energy conversion and storage, Innov. Mater. 2 (2024) 23–100060, https://doi.org/10.59717/j.xinn-mater.2024.100060.
[117] Z. Chen, X. Duan, W. Wei, S. Wang, B.-J. Ni, Recent advances in transition metal-based electrocatalysts for alkaline hydrogen evolution, J. Mater. Chem. A 7 (2019) 14971–15005, https://doi.org/10.1039/C9TA03220G.
[118] T.R. Paudel, A. Zakutayev, S. Lany, M. d'Avezac, A. Zunger, Doping rules and doping prototypes in A2BO4 spinel oxides, Adv. Funct. Mater. 21 (2011) 4493–4501, https://doi.org/10.1002/adfm.201101469.
[119] X. Kang, X.-H. Tan, N. Han, J.-F. Hou, C.-M. Yao, Z.-J. Chen, B.-J. Ni, Tungsten pnictides for water electrolysis: advances and perspectives, Tungsten 6 (2024) 675–695, https://doi.org/10.1007/s42864-024-00268-y.
[120] Z. Chen, N. Han, W. Wei, D. Chu, B.-J. Ni, Dual doping: an emerging strategy to construct efficient metal catalysts for water electrolysis, EcoEnergy 2 (2024) 114–140, https://doi.org/10.1002/ece2.29.
[121] X. Zheng, S. Ding, M. Zhu, F. Ma, J. Hao, S. Lu, F. Duan, M. Du, C. Wang, H. Zhu, Surface doping of cobalt nanoparticles by selenium anion to steer the selectivity in electrocatalytic nitrate reduction, Sustain. Energy Fuel 8 (2024) 4192–4198, https://doi.org/10.1039/D4SE00833B.
[122] R. Deng, M. Guo, C. Wang, Q. Zhang, Recent advances in cobalt phosphide-based materials for electrocatalytic water splitting: from catalytic mechanism and synthesis method to optimization design, Nano Mater. Sci. 6 (2024) 139–173, https://doi.org/10.1016/j.nanoms.2022.04.003.
[123] X. He, Z. Li, J. Yao, K. Dong, X. Li, L. Hu, S. Sun, Z. Cai, D. Zheng, Y. Luo, B. Ying, M.S. Hamdy, L. Xie, Q. Liu, X. Sun, High-efficiency electrocatalytic nitrite reduction toward ammonia synthesis on CoP@TiO2 nanoribbon array, iScience 26 (2023) 107100, https://doi.org/10.1016/j.isci.2023.107100.
[124] J. Gao, B. Jiang, C. Ni, Y. Qi, X. Bi, Enhanced reduction of nitrate by noble metal-free electrocatalysis on P doped three-dimensional Co3O4 cathode: mechanism exploration from both experimental and DFT studies, Chem. Eng. J. 382 (2020) 123034, https://doi.org/10.1016/j.cej.2019.123034.
[125] J.-L. Fan, S.-B. Liu, M.-L. Chen, Z. Wu, S.-P. Sun, Y.-Y. Lou, Electrochemical reduction of nitrate to ammonia on ultra-stable amorphous co–P electrocatalyst, J. Mater. Chem. A 12 (2024) 20077–20087, https://doi.org/10.1039/D4TA02299H.
[126] W. Li, P. Wang, P. Wang, H. Liu, C. Wu, Y. Liu, J. Huang, Z. Fang, H. Guo, Y. Zhang, F. Li, T. Wu, X. Sun, Octahedral CoS2 electrocatalysts for efficient nitrate reduction to ammonia, Inorg. Chem. Front. 11 (2024) 7118–7125, https://doi.org/10.1039/D4QI01632G.
[127] L. Xie, S. Sun, L. Hu, J. Chen, J. Li, L. Ouyang, Y. Luo, A.A. Alshehri, Q. Kong, Q. Liu, X. Sun, In situ derived Co2B Nanosheet Array: a high-efficiency Electrocatalyst for ambient Ammonia synthesis via nitrate reduction, ACS Appl. Mater. Interfaces 14 (2022) 49650–49657, https://doi.org/10.1021/acsami.2c12175.
[128] M. Zhang, Z. Zhang, S. Zhang, Z. Zhuang, K. Song, K. Paramaiah, M. Yi, H. Huang, D. Wang, Efficient electrochemical nitrate reduction to Ammonia driven by a few nanometer-confined built-in electric field, ACS Catal. 14 (2024) 10437–10446, https://doi.org/10.1021/acscatal.4c02317.
[129] J. Zhang, T. Quast, B. Eid, Y.-T. Chen, R. Zerdoumi, S. Dieckhöfer, J.R. C. Junqueira, S. Seisel, W. Schuhmann, In-situ electrochemical reconstruction and modulation of adsorbed hydrogen coverage in cobalt/ruthenium-based catalyst boost electroreduction of nitrate to ammonia, Nat. Commun. 15 (2024) 8583, https://doi.org/10.1038/s41467-024-52780-x.
[130] Q. Wang, Y. Lei, D. Wang, Y. Li, Defect engineering in earth-abundant electrocatalysts for CO_2 and N_2 reduction, Energy Environ. Sci. 12 (2019) 1730–1750, https://doi.org/10.1039/C8EE03781G.
[131] Z. Chen, W. Wei, Y. Shen, B.-J. Ni, Defective nickel sulfide hierarchical structures for efficient electrochemical conversion of plastic waste to value-added chemicals and hydrogen fuel, Green Chem. 25 (2023) 5979–5988, https://doi.org/10.1039/D3GC01499A.
[132] Y. Dong, S. Zhang, X. Du, S. Hong, S. Zhao, Y. Chen, X. Chen, H. Song, Boosting the electrical double-layer capacitance of graphene by self-doped defects through ball-milling, Adv. Funct. Mater. 29 (2019) 1901127, https://doi.org/10.1002/adfm.201901127.
[133] G. Zhang, J. Wang, Z. Wu, R. Shi, W. Ouyang, A. Amini, B.N. Chandrashekar, N. Wang, C. Cheng, Shape-dependent defect structures of monolayer MoS2 crystals grown by chemical vapor deposition, ACS Appl. Mater. Interfaces 9 (2017) 763–770, https://doi.org/10.1021/acsami.6b13777.
[134] G. Xin, H. Sun, S.M. Scott, T. Yao, F. Lu, D. Shao, T. Hu, G. Wang, G. Ran, J. Lian, Advanced phase change composite by thermally annealed defect-free graphene for thermal energy storage, ACS Appl. Mater. Interfaces 6 (2014) 15262–15271, https://doi.org/10.1021/am503619a.
[135] X. Leng, Y. Wang, F. Wang, Alcohols assisted hydrothermal synthesis of defect-rich MoS2 and their applications in humidity sensing, Adv. Mater. Interfaces 6 (2019) 1900010, https://doi.org/10.1002/admi.201900010.
[136] Y. Chen, J. He, H. Pang, P. Jiang, F. Qu, D. Yu, J. Zhang, New insight into electrochemical denitrification using a self-organized nanoporous VO-Co3O4/co cathode: plasma-assistant oxygen vacancies catalyzed efficient nitrate reduction, Sci. Total Environ. 850 (2022) 157845, https://doi.org/10.1016/j.scitotenv.2022.157845.
[137] Z. Deng, C. Ma, Z. Li, Y. Luo, L. Zhang, S. Sun, Q. Liu, J. Du, Q. Lu, B. Zheng, X. Sun, High-efficiency electrochemical nitrate reduction to Ammonia on a Co3O4 Nanoarray catalyst with cobalt vacancies, ACS Appl. Mater. Interfaces 14 (2022) 46595–46602, https://doi.org/10.1021/acsami.2c12772.
[138] J. Chen, F. Wang, X. Qi, H. Yang, B. Peng, L. Xu, Z. Xiao, X. Hou, T. Liang, A simple strategy to construct cobalt oxide-based high-efficiency electrocatalysts with oxygen vacancies and heterojunctions, Electrochim. Acta 326 (2019) 134979, https://doi.org/10.1016/j.electacta.2019.134979.
[139] Z. Chen, G.-F. Han, A. Mahmood, J. Hou, W. Wei, H. Kyong Shon, G. Wang, T. David Waite, J.-B. Baek, B.-J. Ni, Mechanosynthesized electroactive materials for sustainable energy and environmental applications: a critical review, Prog. Mater. Sci. 145 (2024) 101299, https://doi.org/10.1016/j.pmatsci.2024.101299.
[140] F. Yang, Y. Ding, J. Tang, S. Zhou, B. Wang, Y. Kong, Oriented surface decoration of (co-Mn) bimetal oxides on nanospherical porous silica and synergetic effect in biomass-derived 5-hydroxymethylfurfural oxidation, Mol. Catal. 435 (2017) 144–155, https://doi.org/10.1016/j.mcat.2017.03.034.
[141] J. Teng, J.-H. Xu, W.-X. Sun, X.-F. Liu, X. Xu, G.-S. Liu, Single-atom catalysis for advanced oxidation and reduction systems in water decontamination, Rare Metals 43 (2024) 3576–3606, https://doi.org/10.1007/s12598-024-02709-6.
[142] M. Lao, P. Li, Y. Jiang, H. Pan, S.X. Dou, W. Sun, From fundamentals and theories to heterostructured electrocatalyst design: an in-depth understanding of alkaline hydrogen evolution reaction, Nano Energy 98 (2022) 107231, https://doi.org/10.1016/j.nanoen.2022.107231.
[143] C. Wang, J. Li, F. Besenbacher, R. Su, Heterogeneous electrocatalytic synthesis of nitrogenous organic compounds using inorganic nitrogen sources, Nano Mater. Sci. (2024), https://doi.org/10.1016/j.nanoms.2024.10.010. S2589965124001582.
[144] Y. Yu, C. Wang, Y. Yu, Y. Wang, B. Zhang, Promoting selective electroreduction of nitrates to ammonia over electron-deficient co modulated by rectifying Schottky contacts, Sci. China Chem. 63 (2020) 1469–1476, https://doi.org/10.1007/s11426-020-9795-x.
[145] J. Feng, X. Wang, H. Pan, In-situ reconstruction of catalyst in Electrocatalysis, Adv. Mater. 36 (2024) 2411688, https://doi.org/10.1002/adma.202411688.
[146] H. Meng, Z. Chen, J. Zhu, B. You, T. Ma, W. Wei, S. Vernuccio, J. Xu, B.-J. Ni, In situ amorphization of electrocatalysts, Adv. Funct. Mater. 34 (2024) 2405270, https://doi.org/10.1002/adfm.202405270.
[147] Z. Chen, R. Zheng, T. Bao, T. Ma, W. Wei, Y. Shen, B.-J. Ni, Dual-doped nickel sulfide for electro-upgrading polyethylene terephthalate into valuable chemicals and hydrogen fuel, Nano-Micro Lett. 15 (2023) 210, https://doi.org/10.1007/s40820-023-01181-8.
[148] W. Zhu, F. Yao, Q. Wu, Q. Jiang, J. Wang, Z. Wang, H. Liang, Weakened d–p orbital hybridization in in situ reconstructed Ru/β-co(OH)2 heterointerfaces for accelerated ammonia electrosynthesis from nitrates, Energy Environ. Sci. 16 (2023) 2483–2493, https://doi.org/10.1039/D3EE00371J.
[149] W. Zhu, X. Zhang, F. Yao, R. Huang, Y. Chen, C. Chen, J. Fei, Y. Chen, Z. Wang, H. Liang, A hydrazine-nitrate flow battery catalyzed by a bimetallic RuCo Precatalyst for wastewater purification along with simultaneous generation of Ammonia and electricity, Angew. Chem. Int. Ed. 62 (2023) e202300390, https://doi.org/10.1002/anie.202300390.
[150] Y. You, H. Chen, J. Guo, Z. Feng, J. Zhan, F. Yu, L.-H. Zhang, Structure reconstruction driven by oxygen vacancies forming P-CoMoO4/co(OH)2 heterostructure boosting electrocatalytic nitrate reduction to ammonia, Appl. Catal. B Environ. Energy 363 (2025) 124837, https://doi.org/10.1016/j.apcatb.2024.124837.
[151] L. Qiao, D. Liu, A. Zhu, J. Feng, P. Zhou, C. Liu, K.W. Ng, H. Pan, Nickel-facilitated in-situ surface reconstruction on spinel Co3O4 for enhanced electrochemical nitrate reduction to ammonia, Appl. Catal. B Environ. 340 (2024) 123219, https://doi.org/10.1016/j.apcatb.2023.123219.

[152] Q. Gong, H. Zhao, W.-D. Zhang, J.-D. Feng, Y. Zhang, Y. Zhang, J. Liu, B. Liu, J. Zhang, X. Yang, J. Wang, X. Yan, Unveiling the surface reconstruction of CoWO4 on electrocatalytic nitrate reduction reaction, Chem. Eng. J. 504 (2025) 158819, https://doi.org/10.1016/j.cej.2024.158819.
[153] K. Yang, S.-H. Han, C. Cheng, C. Guo, T. Li, Y. Yu, Unveiling the reaction mechanism of nitrate reduction to Ammonia over cobalt-based Electrocatalysts, J. Am. Chem. Soc. 146 (2024) 12976–12983, https://doi.org/10.1021/jacs.3c13517.
[154] J. Chen, L. Ren, X. Chen, Q. Wang, C. Chen, J. Fan, S. Wang, V. Binas, S. Shen, Well-defined nanostructures of high entropy alloys for electrocatalysis, Exploration (2024) 20230036, https://doi.org/10.1002/EXP.20230036.
[155] Z. Chen, T. Ma, W. Wei, W.-Y. Wong, C. Zhao, B.-J. Ni, Work function-guided Electrocatalyst design, Adv. Mater. 36 (2024) 2401568, https://doi.org/10.1002/adma.202401568.
[156] G. Wang, Z. Chen, W. Wei, B.-J. Ni, Electrocatalysis-driven sustainable plastic waste upcycling, Electron 2 (2024) e34, https://doi.org/10.1002/elt2.34.
[157] X.-H. Wang, Q.-L. Hong, L.-Y. Shao, Q.-G. Zhai, Y.-C. Jiang, X. Ai, Y. Chen, S.-N. Li, Copper–nickel oxide nanosheets with atomic thickness for high-efficiency sulfur ion electrooxidation assisted nitrate electroreduction to ammonia, Adv. Funct. Mater. 34 (2024) 2408834, https://doi.org/10.1002/adfm.202408834.
[158] J. Xie, J. Ma, S. Zhao, T.D. Waite, Flow anodic oxidation: towards high-efficiency removal of aqueous contaminants by adsorbed hydroxyl radicals at 1.5 V vs SHE, Water Res. 200 (2021) 117259, https://doi.org/10.1016/j.watres.2021.117259.
[159] D. Li, S. Chen, J. Duan, Decoupling *H supply for industrial nitrate electroreduction coupled with glycerol oxidation, Chem Catal. 3 (2023) 100656, https://doi.org/10.1016/j.checat.2023.100656.
[160] Z. Chen, W. Wei, B.-J. Ni, Transition metal chalcogenides as emerging electrocatalysts for urea electrolysis, Curr. Opin. Electrochem. 31 (2022) 100888, https://doi.org/10.1016/j.coelec.2021.100888.
[161] S. Zhang, M. Jin, H. Xu, X. Zhang, T. Shi, Y. Ye, Y. Lin, L. Zheng, G. Wang, Y. Zhang, H. Yin, H. Zhang, H. Zhao, An oxygen-coordinated cobalt single-atom electrocatalyst boosting urea and urea peroxide production, Energy Environ. Sci. 17 (2024) 1950–1960, https://doi.org/10.1039/D3EE03399F.
[162] W. He, S. Chandra, T. Quast, S. Varhade, S. Dieckhöfer, J.R.C. Junqueira, H. Gao, S. Seisel, W. Schuhmann, Enhanced nitrate-to-Ammonia efficiency over linear assemblies of copper-cobalt nanophases stabilized by redox polymers, Adv. Mater. 35 (2023) 2303050, https://doi.org/10.1002/adma.202303050.
[163] Y. Liu, J. Wei, Z. Yang, L. Zheng, J. Zhao, Z. Song, Y. Zhou, J. Cheng, J. Meng, Z. Geng, J. Zeng, Efficient tandem electroreduction of nitrate into ammonia through coupling cu single atoms with adjacent Co3O4, Nat. Commun. 15 (2024) 3619, https://doi.org/10.1038/s41467-024-48035-4.
[164] C. Han, L. Sun, S. Han, B. Liu, Stabilizing hydrogen radicals in two-dimensional cobalt-copper mesoporous Nanoplates for complete nitrate reduction Electrocatalysis to Ammonia, Angew. Chem. Int. Ed. 64 (2025) e202416910, https://doi.org/10.1002/anie.202416910.
[165] S. Liang, X. Teng, H. Xu, L. Chen, J. Shi, H* species regulation by Mn-co$(OH)_2$ for efficient nitrate electro-reduction in neutral solution, Angew. Chem. Int. Ed. 136 (2024) e202400206, https://doi.org/10.1002/ange.202400206.
[166] X. Chen, Y. Cheng, B. Zhang, J. Zhou, S. He, Gradient-concentration RuCo electrocatalyst for efficient and stable electroreduction of nitrate into ammonia, Nat. Commun. 15 (2024) 6278, https://doi.org/10.1038/s41467-024-50670-w.
[167] J. Lee, A. Kumar, M.G. Kim, T. Yang, X. Shao, X. Liu, Y. Liu, Y. Hong, A.R. Jadhav, M. Liang, N.Q. Tran, H. Lee, Single-metal-atom dopants increase the Lewis acidity of metal oxides and promote nitrogen fixation, ACS Energy Lett. 6 (2021) 4299–4308, https://doi.org/10.1021/acsenergylett.1c02136.
[168] D.W. Stephan, Frustrated Lewis pairs: from concept to catalysis, Acc. Chem. Res. 48 (2015) 306–316, https://doi.org/10.1021/ar500375j.
[169] L. Yang, C. Wang, Y. Li, W. Ge, L. Tang, J. Shen, Y. Zhu, C. Li, Frustrated Lewis pairs on Zr single atoms supported N-doped TiO2-x catalysts for electrochemical nitrate reduction to Ammonia, Adv. Funct. Mater. 34 (2024) 2401094, https://doi.org/10.1002/adfm.202401094.
[170] Y. Ma, L. Zhang, S. Liu, S. Chen, J. Yu, B. Ding, J. Yan, An electron-coupled Co-Zro_2 nanodot heterojunction electrocatalyst with lewis acid–base site pairs enables high redox reaction kinetics of Li–S batteries, ACS Nano 18 (2024) 21480–21490, https://doi.org/10.1021/acsnano.4c06270.
[171] H. Luo, S. Li, Z. Wu, M. Jiang, M. Kuang, Y. Liu, W. Luo, D. Zhang, J. Yang, Relay catalysis of Fe and co with multi-active sites for specialized division of labor in Electrocatalytic nitrate reduction reaction, Adv. Funct. Mater. 34 (2024) 2403838, https://doi.org/10.1002/adfm.202403838.
[172] L. Sun, V. Reddu, A.C. Fisher, X. Wang, Electrocatalytic reduction of carbon dioxide: opportunities with heterogeneous molecular catalysts, Energy Environ. Sci. 13 (2020) 374–403, https://doi.org/10.1039/C9EE03660A.
[173] L. Sun, C. Dai, T. Wang, X. Jin, Z.J. Xu, X. Wang, Modulating the electronic structure of cobalt in molecular catalysts via coordination environment regulation for highly efficient heterogeneous nitrate reduction, Angew. Chem. Int. Ed. 136 (2024) e202320027, https://doi.org/10.1002/ange.202320027.
[174] Y. Xue, Q. Yu, J. Fang, Y. Jia, R. Wang, J. Fan, A wetting and capture strategy overcoming electrostatic repulsion for Electroreduction of nitrate to Ammonia from low-concentration sewage, Small 20 (2024) 2400505, https://doi.org/10.1002/smll.202400505.
[175] W. Zhong, X. Xiang, P. Chen, J. Su, Z. Gong, X. Liu, S. Zhao, N. Zhang, C. Feng, Z. Zhang, Y. Chen, Z. Lin, Shifting hydrogenation pathway via electronic activation for efficient nitrate electroreduction to ammonia in sewages, Chem Catal. 5 (2025) 101182, https://doi.org/10.1016/j.checat.2024.101182.
[176] G. Zhang, B. Li, Y. Shi, Q. Zhou, W.-J. Fu, G. Zhou, J. Ma, S. Yin, W. Yuan, S. Miao, Q. Ji, J. Qu, H. Liu, Ammonia recovery from nitrate-rich wastewater using a membrane-free electrochemical system, Nat. Sustain. 7 (2024) 1251–1263, https://doi.org/10.1038/s41893-024-01406-7.
[177] J. Gao, Q. Ma, Z. Wang, B.E. Rittmann, W. Zhang, Direct electrosynthesis and separation of ammonia and chlorine from waste streams via a stacked membrane-free electrolyzer, Nat. Commun. 15 (2024) 8455, https://doi.org/10.1038/s41467-024-52830-4.